JMEPEG (2015) 24:2185–2207
DOI: 10.1007/s11665-015-1424-2

1059-9495/$19.00

Aluminum-Based Cast In Situ Composites: A Review

S.L. Pramod, Srinivasa R. Bakshi, and B.S. Murty

(Submitted November 2, 2014; published online February 21, 2015)

In situ composites are a class of composite materials in which the reinforcement is formed within the matrix by reaction during the processing. In situ method of composite synthesis has been widely followed by researchers because of several advantages over conventional stir casting such as fine particle size, clean interface, and good wettability of the reinforcement with the matrix and homogeneous distribution of the reinforcement compared to other processes. Besides this, in situ processing of composites by casting route is also economical and amenable for large scale production as compared to other methods such as powder metallurgy and spray forming. Commonly used reinforcements for Al and its alloys which can be produced in situ are Al_2O_3, AlN, TiB_2, TiC, ZrB_2, and Mg_2Si. The aim of this paper is to review the current research and development in aluminum-based in situ composites by casting route.

Keywords Al_2O_3, AMC, casting, in situ composites, TiB_2, TiC, Mg_2Si, MMC

1. Introduction

Al alloys and Al-matrix composites (AMCs) have received much attention for automobile, aerospace, and structural applications due to their high specific strength and specific stiffness, higher hardness and wear resistance, and good elevated temperature resistance (Ref 1-13). Research on Aluminum-based cast in situ composites started about two decades back, and there has been a significant increase in the research in the last five years. Metal Matrix Composites (MMCs) can be synthesized mainly in two ways; solid state processing and liquid state processing. Composites processed by these techniques suffer from various problems like thermodynamic instability of the reinforcement in the matrix, weak matrix-reinforcement interface, inhomogeneous distribution of reinforcement particles, and lack of good elevated temperature mechanical properties. To overcome these problems, researchers came up with in situ processing of composites. The research on Al-based in situ composites started about two decades ago, and there has been a significant increase in the number of papers in recent years. Figure 1(a) shows the number of publications on Al-based cast in situ composites from 1995 to 2014 produced by casting methods.

In conventional processing of composites, the reinforcement is added to the matrix externally and they are termed as ex situ composites. The reinforcements added are hard particles such as SiC, TiC, TiB_2, ZrB_2, and Al_2O_3 some of which also act as nucleating sites for grain refinement in addition to increasing the strength, hardness, and wear resistance. These reinforcements have high melting points, high hardness and mechanical properties. They act as dispersion strengthening agents and hinder the dislocation motion leading to an improvement in the strength of the composite. These composites are suitable for automobile and aircraft components such as cylinder liners, piston, Clutch, and gear and engine block housing. Al-based composites have been processed by powder metallurgy route (solid state processing) or casting route (liquid state processing). In case of powder metallurgy route, the matrix and reinforcement are mixed together and sintered (ex situ) or the reinforcement is formed by the mechanical alloying or reaction of components during sintering (in situ).

The liquid state processing route is the conventional stir-casting process in which the alloy is melted in the furnace and the reinforcement particles are added in to the melt and stirred for distribution of reinforcement and is an ex situ method. Problems arise when the wettability of the particle with the matrix is low or when fine sized reinforcement needs to be added. In this case, either the particles do not mix with the melt and are rejected or their distribution is not uniform. In order to avoid these problems, a new in situ route of processing has been popular in which the reinforcement is formed inside the matrix due to reaction between one or more components with the matrix. These reinforcements have a very high melting point and good mechanical properties as shown in Table 1. Most of the work has been done on TiB_2 as reinforcement for Al-based in situ composites. TiB_2-reinforced composite processed using the salt reaction route is cost effective, and the TiB_2 also acts as a heterogeneous nucleation site during solidification of Al leading to grain refinement as will be shown in later sections. TiB_2 also has good wettability and is more coherent with the Al matrix. To the best of author's knowledge, a review of Al-based in situ composites prepared by casting techniques is not available so far. Such a review is necessary since casting is one of major production methods used in the industry for Al components. Figure 1(b) shows a pie chart of the percentage of total papers published on different in situ reinforcements.

1.1 Advantages of In Situ Composites

Following are a few advantages of the in situ processes over conventional methods:

- In situ synthesized reinforcement is thermodynamically stable. The reinforcement is formed as an equilibrium pro-

This article is an invited paper selected from presentations at "Innovation in Processing of Light Metals for Transportation Industries: A Symposium in Honor of C. Ravi Ravindran," held during MS&T'14, October 12-16, 2014, in Pittsburgh, Pa., and has been expanded from the original presentation.

S.L. Pramod, Srinivasa R. Bakshi and **B.S. Murty,** Department of Metallurgical and Materials Engineering, Indian Institute of Technology, Madras, Chennai 600036, India. Contact e-mail: murty@iitm.ac.in.

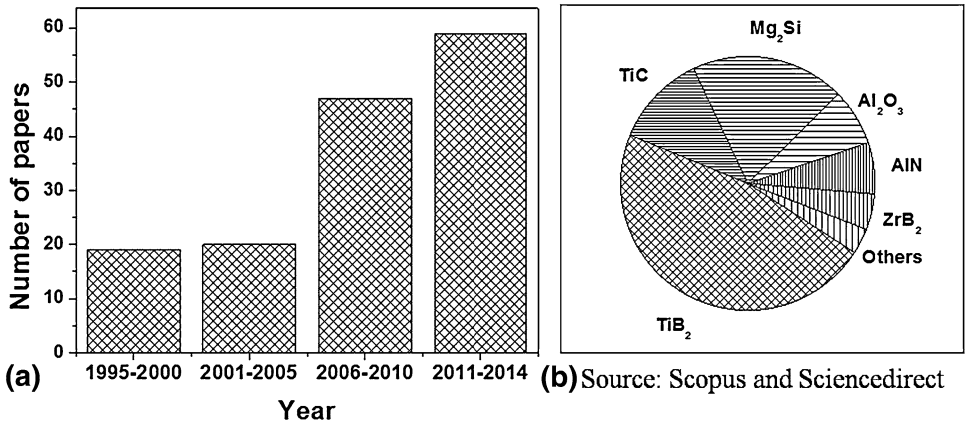

Fig. 1 Number of papers on (a) Al-based cast in situ composites and (b) Various reinforcements

Table 1 Properties of different reinforcements that can be prepared in situ (Ref 14-16)

Reinforcement/properties	TiB_2	TiC	Al_2O_3	ZrB_2	Mg_2Si	AlN
Density, g/cm^3	4.52	4.93	3.99	6.09	1.98	3.26
Melting point, °C	3225	3067	2043	3000	1102	2200
Hardness Vickers, GPa	25-35	24-32	18-21	22-26	4.5	11.8
Elastic modulus, GPa	560	400	400	350	40-50	331
Thermal conductivity, w/m/k	60-120	17-32	30	23	3-8	285
Crystal structure	Hexagonal	Cubic	Hexagonal	Hexagonal	Cubic	Wurtzite

duct of reactions involving the molten alloy matrix and hence is stable during service.

- Less degradation in elevated-temperature services. The wettability of the particle with the matrix is good and because of the clean interface, the bonding between the particle and the matrix is better, which will enhance the high-temperature properties.
- The in situ formed reinforcements are finer in size. Such fine particles are difficult to be added in ex-situ composites as they might choke the feeder.
- The distribution of reinforcement in the matrix is more uniform due to better wettability and stirring during processing.

1.2 Processing of Al-based In Situ Composites

There are several methods by which in situ composites can be synthesized such as melt-elemental/oxide reaction, melt-salt/halide reaction, and melt-gas reaction. The reinforcements that have been produced in situ are TiB_2, TiC, ZrB_2, AlN, Al_2O_3, and Mg_2Si. Most of the literature available on the in situ synthesis of Al-based composite is by the melt-salt/halide reaction, because of the availability of the salt and its cost effectiveness. Al alloys with TiC, TiB_2, and ZrB_2 reinforcements can be prepared by the addition of halide salts. Al_2O_3 and AlN reinforcements can be prepared by the direct melt oxidation and gas-melt reaction, respectively. Mg_2Si in situ composites are formed in situ in Al-Si-Mg alloy during the solidification. In this section, a review of the processing, microstructure, and mechanical properties obtained for each of the in situ reinforcements is presented.

1.3 Al-TiB_2 In Situ Composites

1.3.1 Processing and Microstructure of Al-TiB_2 In Situ Composites. The processing of in situ TiB_2 reinforcement in Al alloys started in early 90s for the preparation of grain refiners. The synthesis of Al-TiB_2 composite using K_2TiF_6 and KBF_4 salt reaction in molten Al was patented by London and Scandinavian Metallurgical Co. Ltd. in 1993 (Ref 17). Many researchers have since synthesized in situ TiB_2-reinforced composites via K_2TiF_6 and KBF_4 salt reaction in Al alloys (Ref 17-23). The TiB_2 particles formed in situ in the Al melt by this method are a few microns in size (Ref 11-13, 18, 20, 24-30). A number of researches have reported the presence of Al_3Ti phase in Al-TiB_2 composites, which is found to degrade the overall mechanical properties of the composite (Ref 31, 32). Later, it was found that Al_3Ti formation can be suppressed by increasing the reaction time and temperature and properly controlling the proportion of salts (Ref 8, 18, 24, 25, 33-37). A schematic diagram of synthesis of A356-TiB_2 composites by this method is shown in Fig. 2.

The reactions between K_2TiF_6 and KBF_4 and molten Al leading to the formation of TiB_2 have been reported by many researchers as follows (Ref 17):

$$3K_2TiF_6 + 13Al \rightarrow 3TiAl_3 + 3KAlF_4 + K_3AlF_6$$

$$2KBF_4 + 3Al \rightarrow AlB_2 + 2KAlF_4$$

$$AlB_2 + TiAl_3 \rightarrow TiB_2 + 4Al$$

It is to be noted that the third reaction being a solid state reaction would happen only when the two particles come in contact. It is more likely that the 2nd and 3rd reaction that happen are as follows:

$$KBF_4 + Al \rightarrow [B] + KAlF_4$$

$$TiAl_3 + 2[B] \rightarrow TiB_2 + 3Al,$$

where [B] refers to B dissolved in molten Al. Mandal et al. (Ref 18) reported the complete formation of TiB_2 without any residual Al_3Ti which was confirmed using XRD analysis of

extracted particles from the composite as shown in Fig. 3. They reported that a melt temperature of 800 °C and reaction time of 1 h with stirring at an interval of 10 min were optimum for synthesis of these composites without any Al_3Ti formation. They also showed that the TiB_2 particles act as heterogeneous nucleation sites in the Al melt and refine the grains. Yue et al. (Ref 38) have reported the thermodynamic calculations for the reaction of K_2TiF_6 and KBF_4 salts in Al melt and found out that ΔG_{TiB_2} is more negative than ΔG_{Al_3Ti} and ΔG_{AlB_2} in the range 430-930 °C suggesting that TiB_2 must form at the expense of Al_3Ti and AlB_2. They also showed that the Gibbs free energy of Al_3Ti increases with increase in temperature and at high temperature, Al_3Ti is not stable and only TiB_2 phase is obtained. The variation in Gibbs free energy for $TiAl_3$, TiB_2 and AlB_2 with increasing temperature is shown in Fig. 4(a) and Table 2.

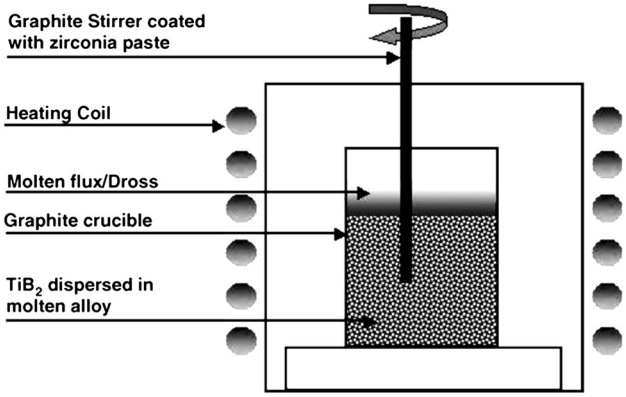

Fig. 2 Schematic diagram for the synthesis of A356-TiB_2 composites (Ref 18)

Table 2 Gibbs free energy for the reactions to form TiB_2 and ZrB_2 (Ref 40)

Reactions	$\Delta G°$, kJ/mol at 727 °C
$2KBF_4 + 3Al = AlB_2 + 2AlF_3 + 2KF$	−404.31
$K_2TiF_6 + 133Al = TiAl_3 + 43AlF_3 + 2KF$	−354.65
$K_2ZrF6 + 133Al = ZrAl_3 + 43AlF_3 + 2KF$	−276.24
$TiAl_3 + AlB_2 = TiB_2 + 4Al$	−101.12
$ZrAl_3 + AlB_2 = ZrB_2 + 4Al$	−77.98

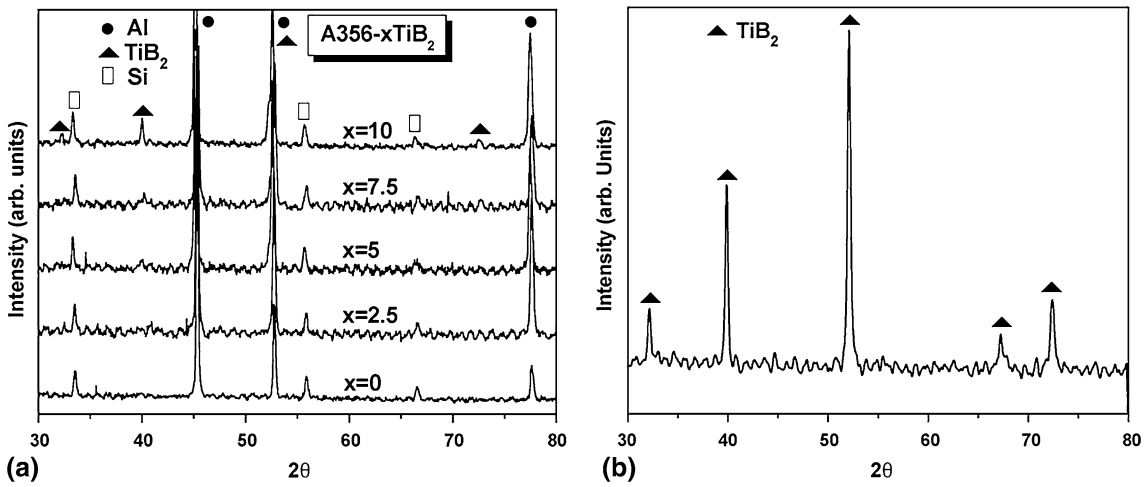

Fig. 3 XRD patterns of (a) A356/TiB_2 MMCs and (b) extracted TiB_2 particles from A356-10 wt.% TiB_2 composite (Ref 18)

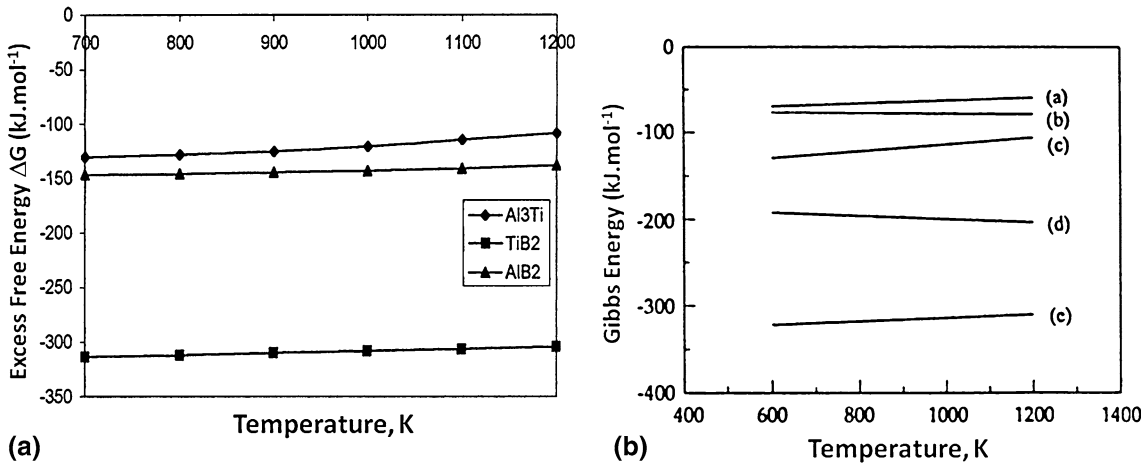

Fig. 4 (a) Variation of excess free energy with temperature for $TiAl_3$, TiB_2 and AlB_2 and (b) standard free energy for possible reactions (Ref 38) (a) $Al + 2B \rightarrow AlB_2$, (b) $Al_3Ti + 2Ti \rightarrow 3TiAl$, (c) $3Al + Ti \rightarrow Al_3Ti$, (d) $Al_3Ti + 2B \rightarrow TiB_2 + 3Al$ and (e)$Ti + 2B \rightarrow TiB_2$ (Ref 39)

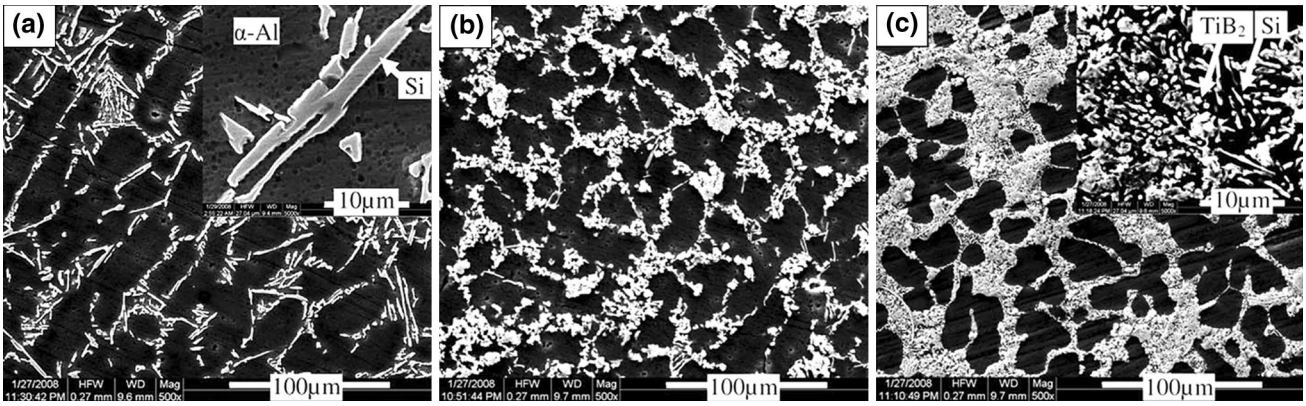

Fig. 5 Microstructure of Al-7Si alloy with (a) 0, (b) 5, and (c)10 wt.% TiB_2 particles and the higher magnification insets in (a) and (c) shows the difference in Si particle size and shape (Ref 11)

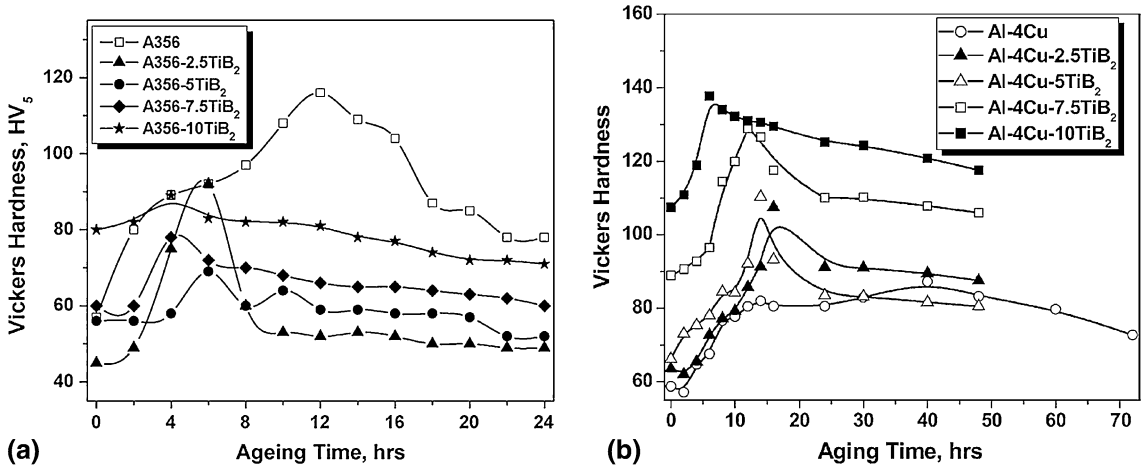

Fig. 6 Hardness of the composites as a function of aging time for A356 and Al-4Cu alloy reinforced TiB_2 composite (Ref 18, 43)

The in situ formed TiB_2 particles reported in many studies are of hexagonal in shape and 0.5-1 μm in size (Ref 11-13, 31, 34). In Al-Si alloys, these TiB_2 particles segregate toward the inter-dendritic region (Ref 11, 12, 22, 26, 33, 36) along with Si and also reduce the eutectic Si length (Ref 26, 33, 36). Kumar et al. (Ref 11) observed significant reduction in eutectic Si length with TiB_2 particle. They have shown that the TiB_2 particles which are segregated to the inter-dendritic region arrest the growth of Si needles. They have observed a thick eutectic mixture of Si and TiB_2 at the grain boundary which increases with the TiB_2 content as shown in Fig. 5.

It has also been found that an increase in the reaction time increases the percentage of TiB_2 (Ref 8, 18, 24, 33, 41-43). Feng et al. (Ref 44) have studied the effect of alloying elements in Al on the dispersion of the TiB_2 particles and found that Si, which also increases the fluidity of Al, improves the dispersion of TiB_2 particles. Kumar et al. (Ref 11, 20, 27) reported that TiB_2 acts as a grain refiner for primary alpha-Al and also modifies the Si in the eutectic mixture. Kumar et al. (Ref 24, 28) and Mandal et al. (Ref 18, 43) have reported an improvement in the aging response with the increase in TiB_2 content in case of A356 and Al-4Cu alloy, respectively, as shown in the aging curves in Fig. 6. The peak aging time for A356 alloy was 12 h while that for the 10 wt.% TiB_2 composite was only 4 h and overaging reduced the hardness of the composite (Ref 18). It is also observed that in case of A356 alloy, the hardness of the composite after aging is lower than the alloy while it is reverse in case of Al-Cu alloys. It has been attributed to the loss of magnesium due to reaction with the K_2TiF_6 and KBF_4 salts in case of A356 alloy, which decreases the amount of Mg_2Si precipitates formed during aging. Chen et al. (Ref 36) have studied the effect of time and temperature on the reaction of K_2TiF_6 and KBF_4 salt with Al to form TiB_2 by holding the melt for 15, 30, 60, and 90 min at 750 to 950 °C and observed increase in TiB_2 content and a more homogeneous distribution with increase in reaction temperature and reaction time. However, Lakshmi et al. (Ref 19) reported that with increase in reaction time beyond 20 min there is a decrease in volume fraction of TiB_2 which is contradictory to the other reports (Ref 8, 18, 24, 33, 41-43).

Murty et al. (Ref 45) synthesized Al-5TiB_2 composite by the addition of K_2TiF_6 and KBF_4 salt at 800 °C and Al-3.45Ti and Al-1.55B master alloy addition at 1000 °C with 60 min reaction time and observed salt addition results in the formation of more Al_3Ti comparing with the master alloy addition. Charbhai et al. (Ref 21) studied the precipitation behavior of Al-4Cu-TiB_2 composite and observed that θ′ phase nucleates preferably on the strain fields of TiB_2 particle/matrix interface and nearby region from the TEM analysis. The precipitation process in composites is faster due to the presence of extensive dislocation network at the TiB_2 particle/matrix interface which acts as potential nucleation sites. Harsha Nandam et al. (Ref 22)

also studied the precipitation kinetics of Al-7Si-0.3Mg-TiB_2 in situ composites synthesized by salt reaction method using Differential Scanning Calorimetry (DSC) and Transmission Electron Microsopy (TEM) and reported faster precipitation kinetics with increase in TiB_2 content. From the DSC data and Kissinger analysis, it was observed that the activation energy for the formation of GP zones in 2.5, 5, and 10 wt.% TiB_2 composites are 83, 67, and 59 kJ/mol, respectively, compared with the base alloy which is 85 kJ/mol (Ref 22).

Al-TiB_{-2} composites can also be synthesized by a self-propagating high-temperature synthesis (SHS) reaction in a Al-Ti-B powder compact/preform added to molten Al (Ref 39, 46-48). Yang et al. (Ref 39) synthesized Al-TiB_2 composites by the addition of Al-Ti-B powder preform to the molten Al at 900 °C and studied the mechanism of formation of TiB_2. They observed that for a Ti:B ratio 1:2 (mole fraction) in the preform, the TiB_2 particulates formed were spherical in shape with a mean size less than 2.0 μm and Al_3Ti particles were also present. To suppress the Al_3Ti phase, a Ti:B ratio 1:4 was required. The reaction sequence of Al-Ti-B preform with Al was also discussed by Yang et al. (Ref 39). They propose that at 660 °C, the Al powder in the preform melts and moves over the surface of Ti powder and reacts to form Al_3Ti phase ($Al(l) + Ti(s) \rightarrow Al_3Ti$). This exothermic reaction partially melts the Al_3Ti phase. The B atoms diffuse in to Al_3Ti and react to form TiB_2 ($Al_3Ti + 2B \rightarrow 3Al + TiB_2$) and liberate more heat. Finally, when the temperature reaches a higher critical value and Ti reacts with B to form TiB_2 ($Ti + 2B \rightarrow TiB_2$). The variation of the Gibbs free energy with temperature for the possible reactions (a) $Al + 2B \rightarrow AlB_2$, (b) $Al_3Ti + 2Ti \rightarrow 3TiAl$,(c) $3Al + Ti \rightarrow Al_3Ti$, (d) $Al_3Ti + 2B \rightarrow TiB_2 + 3Al$ and (e) $Ti + 2B \rightarrow TiB_2$ is shown in Fig. 4(b) indicating that the Gibbs free energy value for TiB_2 formation (d) and (e) is the most negative.

It was proposed that if the molar fraction of Al is larger than 43.5% in Al-Ti-B preform, the TiB_2 particulates will form by a diffusion mechanism, while the TiB_2 particulates will form by a solution-precipitation mechanism the aluminum fraction is lower than 43.5 mol.%. Tee et al. (Ref 46) also synthesized the Al and Al-4Cu with in situ TiB_2 reinforcement by the addition of Al-Ti-B powder compact and performed extrusion of composites and studied their mechanical properties. A few reports have shown that TiB_2 reinforcement in Al alloys can be synthesized with the addition of other compounds. Chen et al. have prepared Al-4.5 Cu-TiB_2in situ composite by the addition of TiO_2, H_3BO_3 and Na_3AlF_6. The TiB_2 particles were found to be hexagonal in shape and distributed uniformly in the matrix with an average particle size of about 0.93 μm. Changizi et al. (Ref 49) fabricated Al-TiB_2 in situ composite by the reaction of TiO_2-H_3BO_3-Na_3AlF_6 with Al. The XRD analysis confirmed the formation of TiB_2, and the particles were spherical with an average diameter of 1 μm and uniformly distributed. The reaction of TiO_2-H_3BO_3-Na_3AlF_6 with Al is given below. Boric acid was used to provide a source of B_2O_3 particles through calcination of the acid.

$$2H_3BO_3 = 3H_2O + B_2O_3$$

$$TiO_2 + B_2O_3 + \frac{10}{3}Al = TiB_2 + \frac{5}{3}Al_2O_3$$

Since the Gibbs free energy of TiB_2 at 1000 °C (-4.2034×10^5 J/mol) is much higher than that of both TiO_2 (-8.7536×10^6 J) and B_2O_3 (-1.4212×10^6 J), the TiB_2 cannot be directly formed by the reaction between B_2O_3 and TiO_2. The Gibbs free energy of Al_2O_3 (-1.8313×10^6 J) is much lower than of both TiO_2 and B_2O_3, and this can be used to reduce the TiO_2 and B_2O_3 with the formation of Al_2O_3 which dissolves in the cryolite.

$$3TiO_2 + B_2O_3 + 6Al = 3Al_2O_3 + 3Ti + 2B$$

$$Ti + 2B = TiB_2$$

$$2Al_2O_3 + 2Na_3AlF_6 = 4AlF_3 + Na_2Al_2O_4 + 2Na_2O$$

The Kirkendall effect in the liquid during the formation of in situ TiB_2 under micro-gravity condition was studied by Anestiev et al. (Ref 50). The experiment was carried out in STS95 space shuttle mission in 1998. Al-B and Al-Ti rods were friction welded, and they are placed in a multi-zone furnace with one side heating source and other side cooling source. The samples were processed at 800 and 900 °C and then quenched. Formation of TiB_2 along with Al_3Ti in the interface of Al-Ti and Al-B rods was reported. The driving force for the shift of Kirkendall plane is diffusion coupled with reaction. Since specimens are in liquid state and gravity effect is not there, the effect of surface tension on the Kirkendall shift is possible.

Functionally graded Al-TiB_2 composite can be processed by centrifugal casting after the synthesis of Al-TiB_2 composite. Forster et al. (Ref 51) fabricated functionally graded Al-TiB_2 composite by centrifugal casting and reported that the TiB_2 particulate content was concentrated toward the outer radius with a clear interface between this region and the remaining unreinforced aluminum matrix. Kumar et al. (Ref 27) fabricated functionally graded A356 and Al-4Cu alloy TiB_2 composite by centrifugal casting. Higher volume fraction of TiB_2 in the outer and inner periphery of the casting was reported. The stirring of the melt before pouring resulted in the dense TiB_2 being segregated to the outer periphery of the casting. In the absence of stirring, the particles settle down in the crucible and the alloy that is first poured into the mold has lower TiB_2 content and solidifies from outer periphery inwards, thus leading to particles being segregated to the interior of the centrifugal casting.

The TiB_2 particles usually get agglomerated in the Al-TiB_2 composite which has been addressed by some methods such as ultrasonic vibration (Ref 52-54) during the processing, ECAP (Ref 26) of composite, re-melting and dilution of composite (Ref 55), rolling in mushy state or room temperature or at high temperature (Ref 28, 56, 57), squeeze casting (Ref 58) and extrusion at room temperature and high temperature (Ref 46-48). Stir casting can help some extent to distribute the particles. In order to avoid agglomeration of TiB_2 particles and porosity and to suppress Al_3Ti formation, ultrasonic vibration technique is used along with conventional stir casting (Ref 54). Individual TiB_2 particles are peeled off from the clusters and then distributed uniformly in the matrix with high intensity ultrasonic vibration. Long rod-like Al_3Ti particles could be broken up into block-like morphology smaller than 10 μm in size which is a reduction in size by 20 times. Porosity can also be reduced by 6 times with ultrasonic vibration (Ref 59). Dengbin et al. (Ref 52) also used high intensity ultrasonic vibration for the synthesis of TiB_2 in situ composite by the addition of K_2TiF_6 and KBF_4 salts and observed in situ TiB_2 nano-particles formation with size between 80 and 120 nm with a good distribution. Ravi et al. (Ref 26) carried out Equal channel angular pressing (ECAP) of in situ Al-5wt.% TiB_2 composite at room temperature for four passes and showed an improvement in the distribution of TiB_2 and observed grain refinement to sub-micron sizes.

1.3.2 Mechanical Properties of Al-TiB_2 In Situ Composites. Mechanical and wear properties of in situ TiB_2-reinforced composites have been extensively studied, and significant improvement has been reported with the increase in wt.% of TiB_2 compared with the base alloy. During the processing of composites, dislocations are developed due to differences in coefficient of thermal expansion between matrix and reinforcement particles. When the composite is subjected to stress, these reinforcement particles act as barriers to the movement of dislocation, and dislocation movement is possible at stress levels much higher than those required to move through matrix phase. Thus, more loads are required for the nucleation of voids and their propagation, leading to higher tensile strength of the composite.

Mandal et al. have shown that Al-4Cu alloy reinforced with 10 wt.% TiB_2 shows a 150% increment in (290 MPa) UTS, 113% increment in yield strength (230 MPa), 100% increment in hardness (86 HV_5), and a 100% reduction in grain size compared to Al-4Cu alloy (Ref 43). They also have shown that the mechanical properties of peak-aged condition had a 32% increase in (383 MPa) UTS, 21% increase in yield strength (280 MPa), 60% increase in hardness (138 HV_5) compared with as-cast condition. Chen et al. (Ref 42) reported a UTS of 416 MPa and yield strength of 315 MPa for Al-4.5 Cu-10 vol.% TiB_2 composite. Kumar et al. (Ref 20) have studied the tensile property of Al-7Si alloy reinforced with 5 and 10 wt.% TiB_2 composite and found 20 and 43% improvement in UTS, 85 and 124% improvement in yield strength, 49 and 108% improvement in hardness.

Yi et al. (Ref 59) have studied the tensile behavior of Al-12Si alloy with 5 wt.% TiB_2 composite and reported 16% increase in UTS at room temperature and 2% reduction at 205 °C when compared with the matrix. Zhao et al. (Ref 60) studied Al-11Si alloy with 2 wt.% TiB_2 composite and showed 40 and 36% increment in UTS and yield strength, respectively, compared with matrix at room temperature and also reported a 23 and 20% improvement in UTS at 250 and 350 °C, respectively. Thus, it is observed that even elevated temperature strength increases by TiB_2 reinforcement. Wang et al. (Ref 55) studied the re-melting and dilution approach to improve the mechanical property by adding Al-5 wt.% TiB_2 master composite in to Al-7Si-0.3Mg, Al-4.5Cu-1.1Si, and Al-6Zn-0.5Mg alloy melt and reported superior improvement in UTS with respect to the conventional halide salt route. Shobha et al. (Ref 33) studied the tensile strength of the 6061-TiB_2 composite and showed an enhancement by 58% at 6 wt.% TiB_2, while hardness enhanced by 47% at 12 wt.% TiB_2. Al 6061-4.98, 9.29, and 13.62 wt.% TiB_2 in situ composites shows an increase of 20, 45, and 50% in UTS and 10, 20, and 28% in hardness, respectively. In addition, the ductility also improved by 14 times with 13.62 wt.% TiB_2(Ref 61). The Al-8Si-10 wt.% TiB_2 shows 44, 125, and 110% improvement in UTS, Yield strength, and hardness, respectively, when compared with matrix.

Tee et al. (Ref 46) studied the extrusion of Al-TiB_2 composite at 350 °C with an extrusion ratio of 12:1 at a rate of 2.85 mm/s. They reported an improvement of up to 61% in tensile strength, 58% in yield strength, and 17% in modulus for 10 vol.% of TiB_2. Tee et al. (Ref 48) also studied the extrusion of Al and Al-4Cu with 15 vol.% TiB_2 at 350 °C with an extrusion ratio of 12:1 at a rate of 2.85 mm/s. The tensile and yield strengths showed a significant improvement by an order of 2 but the ductility of the composites reduced to 68 and 84% for Al and Al-Cu matrix, respectively, with the presence of Al_3Ti phase. They also reported that the wear resistance of Al-10% TiB_2 composite was 18.5 times higher than the unreinforced Al, while the wear resistance of Al-Cu-15 vol.% TiB_2 composite was 3.1 times higher than the unreinforced Al-Cu matrix (Ref 47).

Wang et al. (Ref 62) studied the impact behavior of Al-7Si-0.35Mg-12.5 TiB_2 in situ composite at various temperatures and found the TiB_2 reinforcements decreased the impact toughness of the composite and reported two failure mechanisms of the in situ Al-TiB_2 composite: the eutectic silicon cracking and the "pull-out" of the TiB_2 reinforcement. Wang et al. (Ref 63) also studied the fatigue crack initiation and propagation in A356 alloy reinforced with in situ TiB_2 particles and explained the mechanism. A356-TiB_2 composite exhibits a higher high cycle fatigue life but a faster crack growth rate compared with the unreinforced alloy, suggesting that the composite has a higher resistance to crack initiation but a lower resistance to crack propagation. After initiation, cracks first tend to propagate within the matrix and avoid TiB_2 particles, and there is no cracking in the in situ TiB_2 particles and at high stress intensity, the composite fractures. Wang et al. (Ref 35) reported 33% reduction in grain size, 10% increase in yield strength, 11% increase in UTS observed for A356-8.37 vol.% TiB_2 composite compared with A356 alloy. Also for T6-treated condition, 27% reduction in grain size, 41% increase in yield strength, 20% increase in UTS observed for A356-8.37 vol.% TiB_2 composite compare with T6-treated A356 alloy.

Zhang et al. (Ref 32) have studied the damping behavior of Al-5 wt.% TiB_2 composite with Ti addition and reported the damping capacity of Al-5 wt.% TiB_2 composite is lower with Ti addition compared with the composite without Ti addition. Excess Ti in Al-5 wt.% TiB_2 composite can improve damping capacity at relatively high temperature for it forms a thin layer of Al_3Ti on TiB_2 particulate and decrease damping capacity at low temperature. They show that the damping capacity of Al/TiB_2 composite with 0.1 Ti and 0.4 Mg was higher than that of Al/TiB_2 composite. The better particulate/aluminum interface of Al/TiB_2 composite with Ti and Mg is the cause for improving the damping capacity of Al-5 wt.% TiB_2 composite (Ref 64).

The abrasive wear behavior of Al-4Cu alloy with 5 and 10 wt.% TiB_2 particles was studied by Kumar et al. (Ref 24), and they showed significant improvement of wear property with increase in TiB_2. Mandal et al. (Ref 13) also studied the abrasive wear behavior of in situ formed 2.5, 5, 7.5, and 10 wt.% TiB_2 particles in Al-4Cu alloy. They have reported that the percentage Fe content in wear debris increases with increase in wt.% of TiB_2. The reduction in wear rate of composite was due to the substantial amount of iron rich phases formed from the disk during the wear process which acted like an effective in situ solid lubricant. It is also reported that the delamination of the matrix phase (coarse debris) and removal of the fine TiB_2 particles (fine debris) result in two classes of wear debris. Dry sliding wear behavior of A356-2.5, 5, 7.5, 10 wt.% TiB_2 composites showed that the wear rate was 70% lower at 78.4 N load for 10TiB_2 composite compared with A356 alloy. Mandal et al. (Ref 12) also reported the wear resistance of 150% at lower loads of 39.9 and 58.8 N for 10TiB_2 composite in comparison with A356 alloy. Mandal et al. (Ref 29) studied the wear behavior of Al-12Si alloy reinforced with in situ 10 wt.% TiB_2 particles and showed a 60% reduction in wear rate at 78.4 N load when compared with Al-12Si alloy. They

also observed that the TiB_2 particle reduces the Si particle size and the fine Si particles from the surface and sub-surface cracking resulted in the finer debris (Ref 29).

Kumar et al. (Ref 20) have studied the wear property of Al-7Si alloy reinforced with 5 and 10 wt.% TiB_2 composite and found 36 and 66% improvement in wear properties, respectively, compared with the Al-7Si alloy. The wear rate reduced with increase in wt.% TiB_2. Also the increase in TiB_2 causes more Fe removal from the disk and results in an increase in percentage of Fe in the wear surface with increase in TiB_2 and normal load as shown in Fig. 7. The SEM micrographs of worn surface of Al-7Si alloy and Al-7Si-10TiB_2 composite are shown in Fig. 8. It was observed that Al-7Si alloy on sliding at high load deforms plastically and progressive transfer of material to the counterface, and its re-depostition leads to seizure of matrix Al-7Si alloy. In case of Al-7Si alloy, the wear

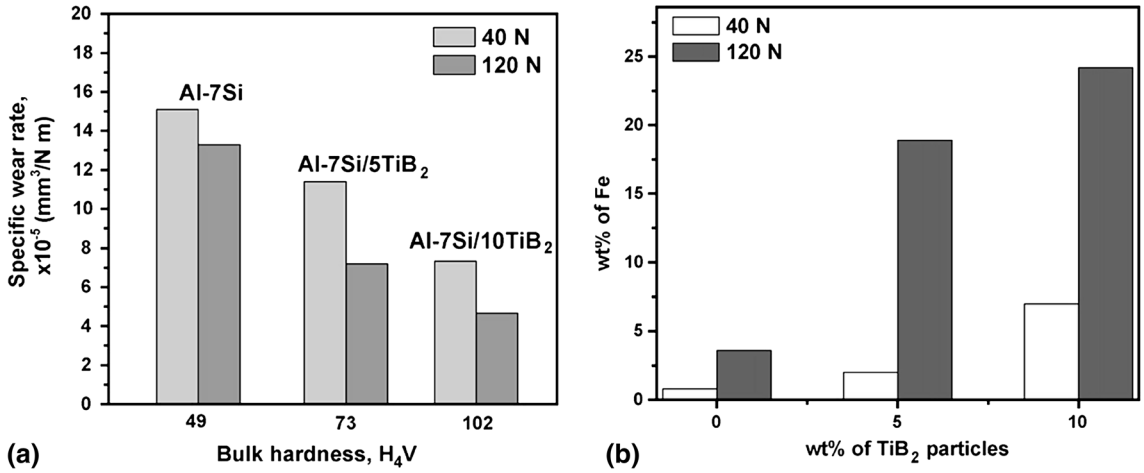

Fig. 7 (a) Specific wear rate of Al-7Si alloy-based composites as a function of load and hardness and (b) average value of Fe content on worn surface measured from EDS as a function of amount of TiB_2 and applied load (Ref 20)

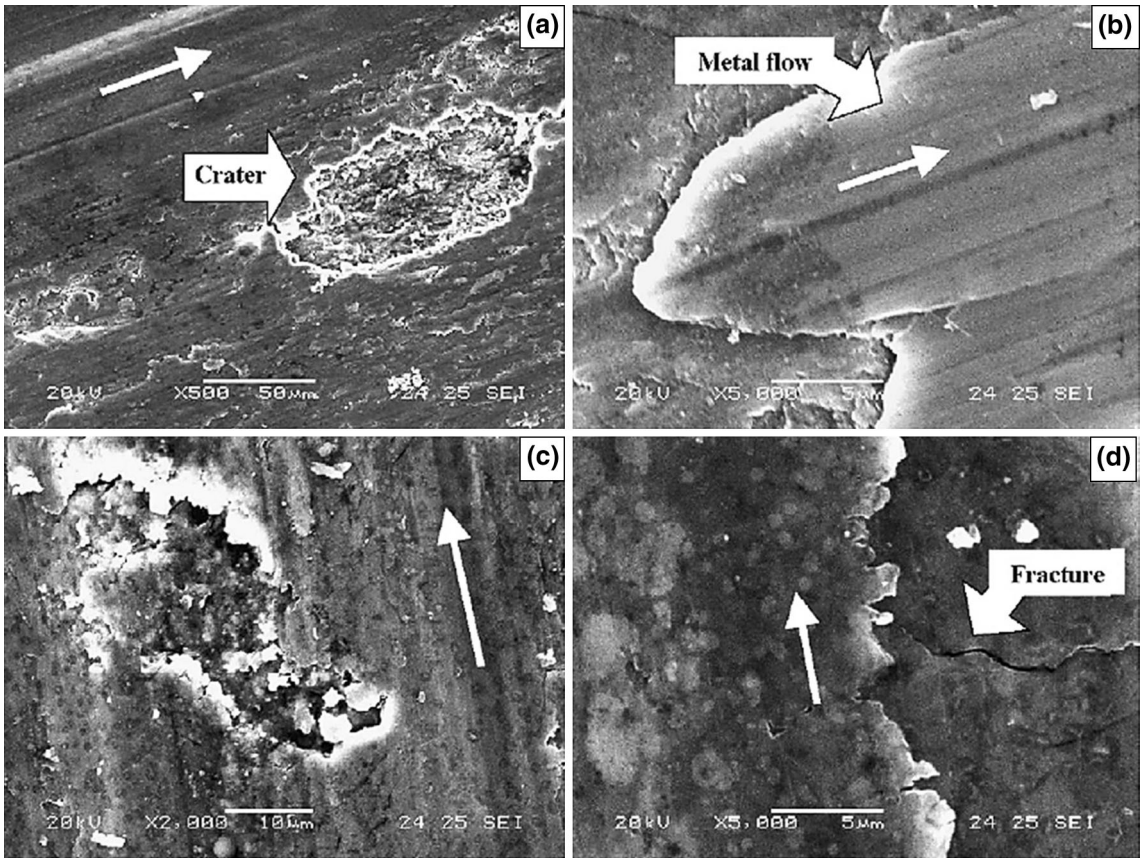

Fig. 8 SEM micrographs of worn surface of (a, b) Al-7Si alloy and (c, d) Al-7Si-10TiB_2 at different magnifications under a normal load of 120 N. The arrow marks show the sliding direction (Ref 20)

mechanism is adhesion and for Al-7Si-10TiB_2 samples, the wear mechanism at high load is by delamination of mechanical mixed layer. The worn surface showed granular nature of shallow crater with an evidence of fracture in transfer layer. The transfer layer on the worn surface of these composites shows a mixture of iron from steel disk along with composite material, which was subsequently removed by delamination caused by craze cracks.

Kumar et al. (Ref 25) also studied the erosion behavior of A356-10 wt.% TiB_2 by design of experiment technique and found out significance of main and interaction factors on erosion rate using analysis of variance (ANOVA). They have explained the erosion mechanism, and at low angles the major wear mechanism for both the A356 alloy and composite was found to be abrasion, while at high angle the wear mechanism is of impact wear. However, the effect of abrasion and impact wear is less for the composite. Kumar et al. (Ref 11) also studied high-temperature wear behavior of Al-7Si-TiB_2in situ composites. The Al-7Si alloy showed transition from mild to severe wear at 80, 60, and 40 N at temperatures of 100, 150, and 200 °C, respectively. The alloy reinforced with 5 wt.% of TiB_2 showed the transition at 120 N and 200 °C, and the transition load decreased to 80 N at 300 °C. The addition of 10 wt.% of TiB_2 showed the transition only at 100 N and 300 °C. At elevated temperatures, the wear mechanism for Al-7Si alloy was adhesion and severe wear, whereas, for composites, oxidation, delamination, and severe wear are predominant. The addition of TiB_2 particles increases the wear resistance properties of Al-7Si alloy even at high temperature. With the addition of 5 and 10 wt.% of in situ TiB_2 particles to the Al-4Cu matrix, the transition temperatures are increased to 200 and 300 °C and the loads are increased to 100 and 120 N, respectively. At elevated temperature, the predominant wear mechanisms for the Al-4Cu alloys are adhesion and metal flow, whereas for Al-4Cu-TiB_2 composites oxidation, delamination, and metal flow are the most dominant wear mechanisms (Ref 30).

Sivaprasad et al. (Ref 65) studied the abrasive and erosive wear behavior of Al 6063-5 and 10 wt.% TiB_2 in situ composites and proposed the mechanism to be a mix-up of micro-cutting, ploughing, and grain pull-out, while for erosion it is found mainly due to plastic deformation and voids. They have also shown an improvement in wear property with increase in TiB_2. Natarajan et al. (Ref 66) studied sliding wear behavior of Al 6063-5, 10 wt.% TiB_2 in situ composites at elevated temperatures and observed 50% improvement in wear resistance with 10 wt.% TiB_2 at 30 N normal load. 40% increase in wear resistance at 100 °C and 50% increase in wear resistance at 200 and 300 °C for TiB_2 composite when compared with Al 6063 alloy.

Kumar et al. (Ref 28) have studied the influence of room temperature and cryogenic temperature rolling on the aging and wear behavior of Al-4Cu-5TiB_2 in situ composites and reported that room and cryogenic temperature rolling and subsequent peak aging of the composite has resulted in an increase in hardness of 25% compared with the as cast and peak aged composite. Ramesh et al. (Ref 67) studied the mechanical and wear behavior of Al 6063-13.12 wt.% TiB_2 composites and showed an increment of 21, 47, and 65% in micro-hardness, UTS and modulus of elasticity, respectively, in comparison with matrix alloy and also showed an increase in ductility for composite due to grain refinement. Al 6063-13.12 wt.% TiB_2 also shows improvement wear rate of 70 and 100% at 50 and 10 N loads, respectively, at sliding velocity of 0.2 m/s for 30 min test duration. For a maximum load of 50 N, 31 and 32% reductions in coefficient of friction and wear rates, respectively, were observed for 10 wt.% TiB_2-reinforced composites when compared with the matrix alloy. The SEM micrograph of the wear track of Al 6063 alloys and composites are shown in Fig. 9. The morphology of worn surfaces of matrix alloy shows wider and shallow grooves on the surface, whereas fine grooves are noticed in case of composites. Worn surfaces also show the presence of some agglomerated wear debris which is oriented in the direction of sliding. The debris is a mixture of matrix material and steel counterface and it includes fractured TiB_2 particles. Since the hardness of the counter body is lower than TiB_2 particles, micro-ploughing is dominant wear mechanism in case of the composites and it is evident from the worn surfaces of the composites with higher TiB_2 content.

Niranjan et al. (Ref 8) studied the dry sliding wear behavior of A356-6 wt.% of TiB_2 composite and explained the improvement in wear resistance due to strong particle/matrix bonding in Al/TiB_2 composites, which enables the in situ particles to be retained in the wear surface during sliding, thereby effectively resisting the shear deformation. Rajan et al. (Ref 34) studied the wear behavior of AA7075 Al alloy reinforced with TiB_2 composite and the wear mode was observed to be abrasive at room temperature and metal flows at high temperature and the samples show severe wear beyond 180 °C. At room temperature, TiB_2 particles reduced the cutting and plastic deformation. Xue et al. (Ref 58) studied the dry sliding wear behavior of gravity-cast and squeeze-cast Al 2014 alloys and in situ 5 vol.% of TiB_2 composites. The coefficients of friction of the squeeze-cast alloy and composite both decrease as the applied load was increased. In the case of the squeeze-cast alloy, a larger quantity of Fe is generated in the wear debris compared with that of the gravity-cast alloy due to the high hardness. In the case of the squeeze-cast composite, more Fe is formed in the wear debris compared with that of the gravity-cast composite due to the fact that the higher matrix hardness and the dispersed TiB_2 particles scratch and wear away the counter-face steel disk. The Fe-rich phase can act as an effective in situ solid lubricant, thereby aiding in reducing the wear rates of the squeeze-cast alloy and composite.

The in situ TiB_2-reinforced Al matrix composites showed significant improvement in mechanical properties compared with the matrix. Researchers have showed increase in UTS and YS with increase in wt.% of TiB_2 reinforcement (Fig. 10). The improvement of UTS and YS for Al-Si alloys is due to the refinement of α-Al, reduction in particle size of eutectic Si with the addition of TiB_2, and hardening due to TiB_2 particles. Si needles in Al-Si alloy act as stress raisers but the addition of TiB_2 results in reduction of size of eutectic Si and results higher strength. The eutectic Si and TiB_2 will form a network structure in the inter-dendritic in-case of hypo-eutectic Si alloys and will restrict the dislocation movement and crack growth leads to the improvement in mechanical properties. Other Al alloys also showed improvement in mechanical properties because of grain refinement of α-Al and hardening due to TiB_2 reinforcement. The particle distribution also plays a vital role in the mechanical properties of the composites. Few researchers reported not much increase in mechanical properties with TiB_2 reinforcement or reduction in mechanical property with increase in TiB_2, due to the agglomeration of TiB_2 particles.

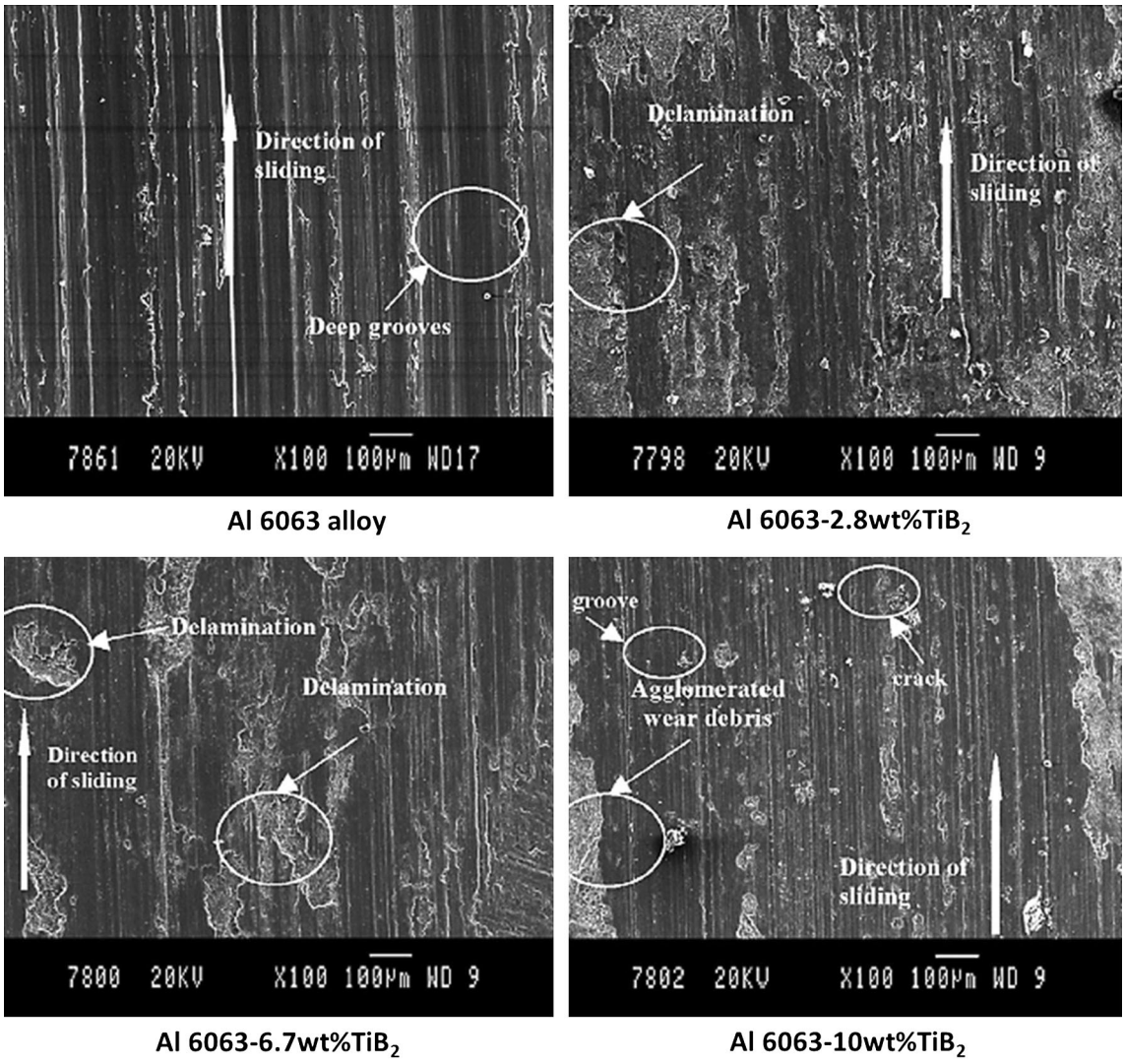

Fig. 9 SEM micrographs of wear tracks of Al 6063 alloy and Al 6063-TiB_2 in situ composites at a load of 10 N and sliding velocity of 0.209 m/s (Ref 67)

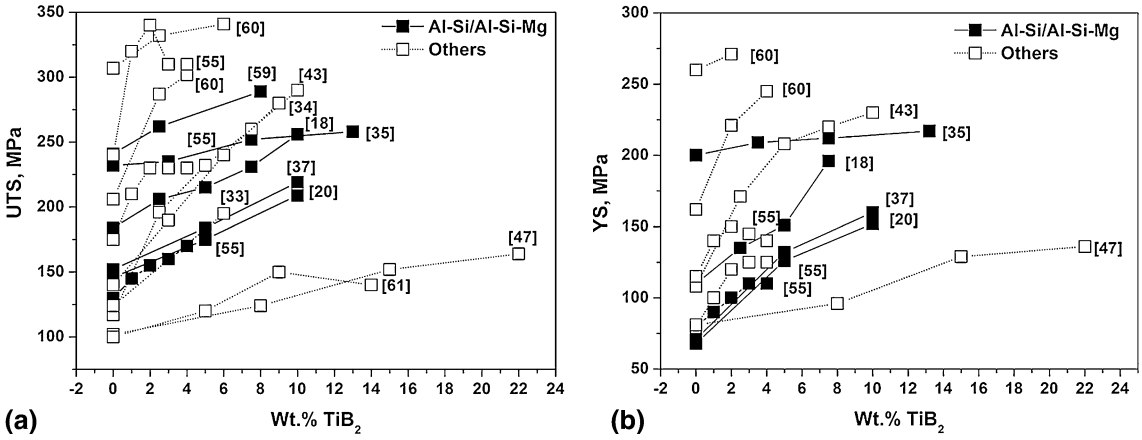

Fig. 10 (a) UTS and (b) yield strength for Al-TiB_2 in situ composites (References are shown in brackets)

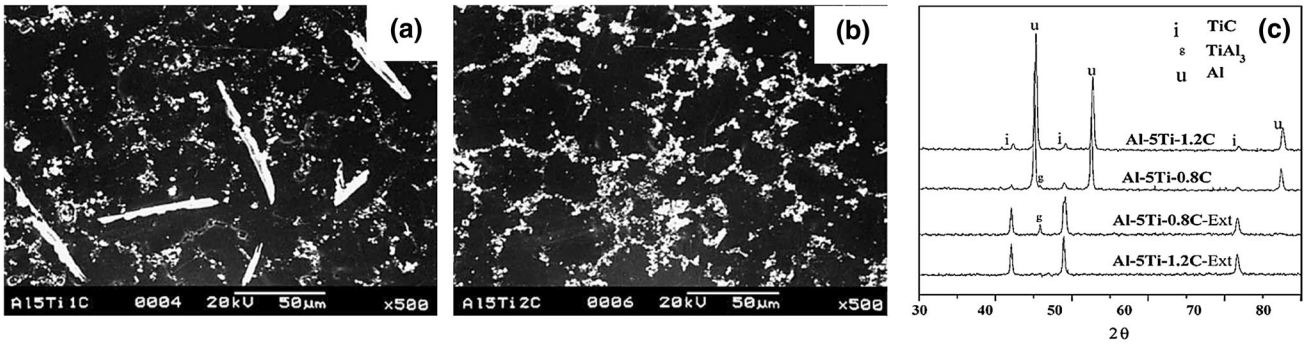

Fig. 11 SEM photomicrograph of (a) Al-5Ti-0.8C master alloy containing $TiAl_3$ and TiC particles in Al matrix, (b) Al-5Ti-1.2C master alloy containing only TiC particles in Al matrix and (c) XRD patterns of Al-5Ti-0.8C and Al-5Ti-1.2C master alloys and those of extracted TiC particles (Ref 23)

1.4 Al-TiC In Situ Composites

TiC particles can be synthesized in situ by several ways such as salt reaction with the molten Al, addition of Al-Ti-C powder compact or by the reaction of CH_4 gas with the melt. Vinod Kumar et al. (Ref 23) developed Al-5Ti-0.8C and Al-5Ti-1.2C master alloys with TiC particles for the grain refinement of Al-7Si alloy. These Al-Ti-C composites (master alloys) were developed by the reaction of molten Al melt with K_2TiF_6 and graphite. They could demonstrate suppression of Al_3Ti and formation of only TiC by proper control of reaction temperature, time, and proportion of K_2TiF_6 and graphite added. SEM micrograph and XRD analysis of Al-5Ti-0.8C and Al-5Ti-1.2C addition in Al are shown in Fig. 11. In the case of Al-5Ti-0.8C, observed the presence of $TiAl_3$, whereas for Al-Al-5Ti-1.2C no $TiAl_3$ particles could be detected. Vinod kumar et al. (Ref 23) studied the grain refinement of Al-7Si alloy with the addition of Al-5Ti-0.8C and Al-5Ti-1.2C master alloy and observed significant improvement in grain refinement byTiC.

Birol et al. (Ref 68) have synthesized Al-TiC in situ composite by K_2TiF_6 and graphite powder addition to Al melt at 1000 °C. It was observed that with the increase in reaction time of 1, 5, 10, and 20 min, the Al_3Ti phase fraction reduced along with an increase in TiC phase.

The reaction sequence between K_2TiF_6 and graphite powder leading to TiC formation is as follows:

$$3K_2TiF_6 + 4Al \rightarrow 3Ti + 3KAlF_4 + K_3AlF_6$$

$$Ti + 3Al \rightarrow Al_3Ti$$

$$Al_3Ti + C \rightarrow TiC + 3Al$$

Bauri et al. (Ref 69) also have optimized parameters for the complete formation of TiC in Al without the Al_3Ti phase. Al-TiC in situ composites were processed at different temperatures from 700 to 1200 °C, and it was observed that the blocky-type Al_3Ti phase formed at temperatures less than 1000 °C. At 1200 °C, there was no evidence of Al_3Ti formation after a reaction time of 30 min. Sharma et al. have synthesized Al-3Ti-0.75C master alloy grain refiner using K_2TiF_6 and graphite addition at three different reaction temperatures 800, 1100, and 1200 °C and reaction times of 5, 15, 30, 40, and 60 min and reported complete formation of TiC at 1100 and 1200 °C (Ref 70). Al-12Si-10 wt.% TiC in situ composites have also been prepared by direct reaction of Ti and activated charcoal in molten Al alloy at 1200 °C for 30 min reaction time (Ref 71). The composite was casted in to plates friction stir butt welding was carried out. The TiC particles were observed to be very finely distributed in the stir zone accompanied by grain refinement (Ref 71).

Rai et al. (Ref 72) also synthesized Al-10TiC in situ composite by the reaction of molten Al with K_2TiF_6 and graphite powder at 1200 °C. The SEM micrograph and the XRD analysis of composite and extracted particles show the presence of TiC, and the TiC particles were segregated toward the grain boundary. Rolling and forging were carried out to de-agglomerate and re-distribute the TiC particles, and it was found that the size of the TiC agglomeration was reduced. Hot forging of Al-10TiC showed an increase of 40 and 20% in UTS and yield strength, respectively, compared with Al-3TiC composite. Rolling and forging improved the yield and tensile strengths of Al-TiC composites through the strain hardening mechanism (Ref 72).

Sahoo et al. (Ref 73) synthesized Al-TiC in situ composites by introducing carbon carrying gas, methane (CH_4) in to the Al-Ti melt held in Ar atmosphere. The nucleation of the carbide occurs via titanium diffusing to the carbon containing bubble and precipitating TiC on the surface as carbide via a solid-liquid chemical reaction. The TiC particles were in the size range of 0.1-2.0 µm. Other researchers produced Al-TiC in situ composites with the addition of Ti and C (graphite and activated charcoal) to the melt in the form of powders or compact in to pellets /preforms, which react with the molten Al and form TiC inside the melt (Ref 5, 74-76). Yang et al. have prepared TiC-reinforced Al-20Si-5Fe alloy composite by Al-Ti-C powder addition in to the melt. The Al-TiC powders were milled and compacted and then added in to the melt. The melt was then spray atomized, and the microstructure was studied (Ref 76).

Li et al. synthesized Al-15 wt.% TiC in situ composites by the self-propagating high temperature synthesis (SHS) reaction between the Al melt and Ti-C powder (Ref 5). Thermodynamic calculations were made for Al-15 wt.% TiC at initial temperatures of aluminum melt T_{melt} = 900 and 1000 °C and at Ti/C molar ratios with and without Al powder. SHS reaction was observed with formation of flashes and sparkling once the powder mixtures were added in to aluminum melt. Excess C powder increases the adiabatic temperature and leads to formation of Al_4C_3 phase, which is considered to be unfavorable in Al-TiC composites. The presence of Al powder in the mixture results in the significant drop in adiabatic temperature.

Ti and C powders with the stoichiometric ratio Ti/C = 1:1 were used for making composites.

Al-4.5 wt.% Cu reinforced by in situ TiC composite was produced by direct reaction between Al-Ti-C perform and the molten alloy at 1000 °C. In situ TiC particles are of spherical shape and 2-3 μm in size, and 60% increase in UTS was observed in comparison with the base alloy (Ref 77). Most of the literature suggest the reaction temperature for the TiC formation is 1000-1200 °C, and the porosity level and other oxide impurities in the melt will be higher at that temperature. Liu et al. (Ref 78) synthesized in situ TiC in Al melt at 750 °C by the addition of Al-Ti-C pellet preheated at 750 °C and the TiC particles formed were spherical in shape and smaller than 1 μm. The XRD pattern (Fig. 12a) shows the formation of TiC along with the Al_3Ti phase. The optical micrographs (Fig. 12b) at low magnification showed the agglomerated TiC particles and at higher magnification show that the particles are spherical in morphology. Al-TiC in situ composite was synthesized by the reaction of SiC and Ti with Al melt (Ref 79). Since SiC is relatively unstable at high temperature and it releases carbon, which reacts with titanium to form TiC leaving free Silicon in the melt. They observed that the wear rate decreases linearly with increase in volume fraction of TiC.

The Al-TiC in situ composites show better mechanical and wear properties compare with the base alloy. Kumar et al. (Ref 80) synthesized Al-4.5% Cu alloy reinforced with 5, 7, and 10 wt.% TiC particles by the addition of Ti and activated charcoal powders and obtained TiC reinforcement with residual Al_3Ti phase. The addition of 5, 7, and 10 wt.% TiC increased the UTS by 14, 32, and 52%, respectively. The coefficient of friction decreased with increasing applied load and TiC reinforcement (Ref 81). The wear resistance enhanced with the increase in TiC reinforcement. Wang et al. (Ref 74) studied the wear behavior of spray-deposited Al 7075 alloy-reinforced TiC composite produced by the reaction of Al-Ti-C preform and observed an increase in wear resistance with increase in wt.% of TiC reinforcement.

The improvement in the hardness is of the order of 2 and 6 for 12 and 18 vol.% TiC respectively, whereas the reduction in wear rate is in the order of 4 and 7 for 12 and 18 vol.% TiC respectively (Ref 79). Al-5 wt.% TiC composite showed 50% increase in hardness and 78% increase in 0.2% proof stress (compressive) (Ref 69). To improve the distribution of TiC in Al-TiC composite, rolling and forging were done which also improved the mechanical properties. Rolling and forging improved the yield and tensile strengths of Al-TiC composites through the strain hardening mechanism and in the case of hot rolling and for hot forging, the strengthening effect was found to be due to recrystallization. The hot-forged samples showed significant improvement in UTS of 140, 170, and 200 MPa for 3, 5, and 10 wt.% TiC composites, respectively, and yield strength did not show much difference (Ref 72). In case of Al-TiC composite, for the pin on disk wear study, at a lower load, with increasing TiC content, the wear rate was decreased. At higher loads, the wear rate increased with increasing TiC due to the worn out TiC particles acting as abrasive particle removing more matrix material (Ref 74). Machinability of Al-TiC in situ composites containing 3, 5, and 10 wt.% TiC produced by the addition of Ti and charcoal powder in to the melt at 1250 °C has been studied by Rai et al. (Ref 82). Higher volume fraction of TiC particles causes discontinuous and favorable chip formation without any build- up edge formation during machining of Al-TiC composites.

1.5 Al-ZrB_2 In Situ Composites

Al-ZrB_2 in situ composites are usually synthesized by the addition of K_2ZrF_6 and KBF_4 salts, which react with molten Al and form ZrB_2 in the melt (Ref 10, 40, 83-86). Various researchers have prepared in situ ZrB_2-reinforced Al alloys, and reported improved mechanical properties and wear resistance. In situ preparation of Al matrix composites reinforced with ZrB_2 and TiB_2 particles has been processed by the addition of KBF_4, K_2ZrF_6 and K_2TiF_6 salts by Zhao et al. (Ref 40). The TiB_2 and ZrB_2 particles are hexagonal in morphology and the average size of TiB_2 and ZrB_2 particles is about 1.0 and 0.30 μm, respectively. XRD analysis and TEM analysis confirmed the formation of TiB_2 and ZrB_2 particles. A 2024 Al alloy composite reinforced with nano ZrB_2 particle has been synthesized by the K_2ZrF_6 and KBF_4 halide reaction inside the molten 2024 alloy (Ref 83). Grain refinement was observed with the increase in the wt.% of 30-100 nm size ZrB_2nano-particles.

The formation of ZrB_2 particles can be explained by the following in situ reactions which take place between Al alloy and KBF_4 and K_2ZrF_6 salts

$$2KBF_4 + 3Al \rightarrow AlB_2 + 2KAlF_4$$

$$3K_2ZrF_6 + 13Al \rightarrow 3Al_3Zr + K_3AlF_6 + 3KAlF_4$$

$$AlB_2 + Al_3Zr \rightarrow ZrB_2 + 4Al$$

From the theoretical calculations, one mole of K_2ZrF_6 and two mole of KBF_4 are required to produce 1 mole of ZrB_2 (Ref 84). Zhao et al. (Ref 40) have suggested the reactions for the formation of TiB_2 and ZrB_2 reinforcement in Al alloy using KBF_4, K_2ZrF_6 and K_2TiF_6 salts along with the Gibbs free

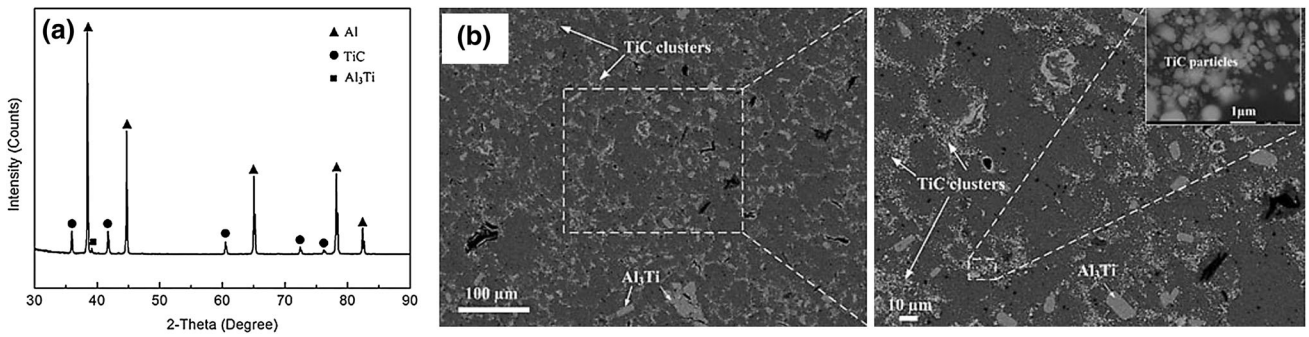

Fig. 12 (a) XRD pattern of Al-TiC composite and (b) optical microstructure of Al-TiC composite at low and higher magnification (Ref 78)

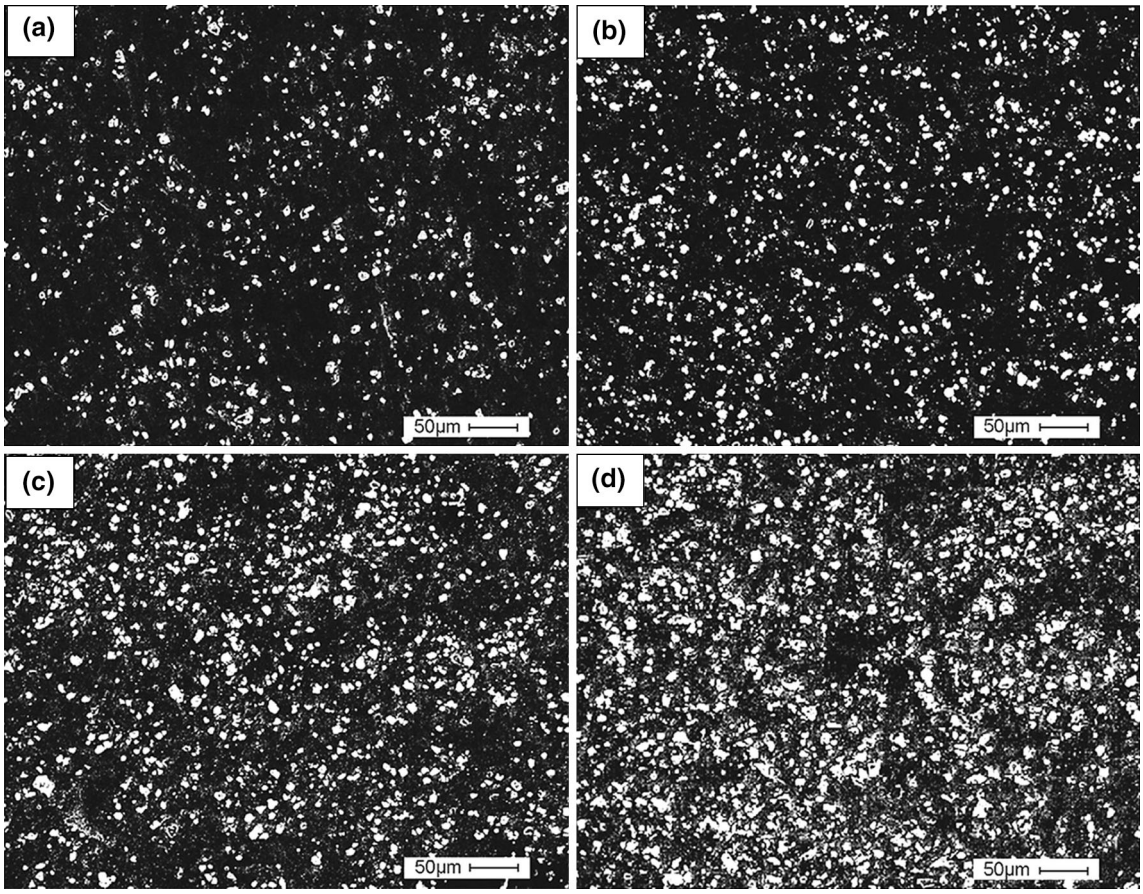

Fig. 13 SEM micrographs of the composites synthesized from Al-x wt.% (K_2ZrF_6-KBF_4) systems. (a) x = 10, (b) x = 15, (c) x = 20 and (d) x = 25 (Ref 86)

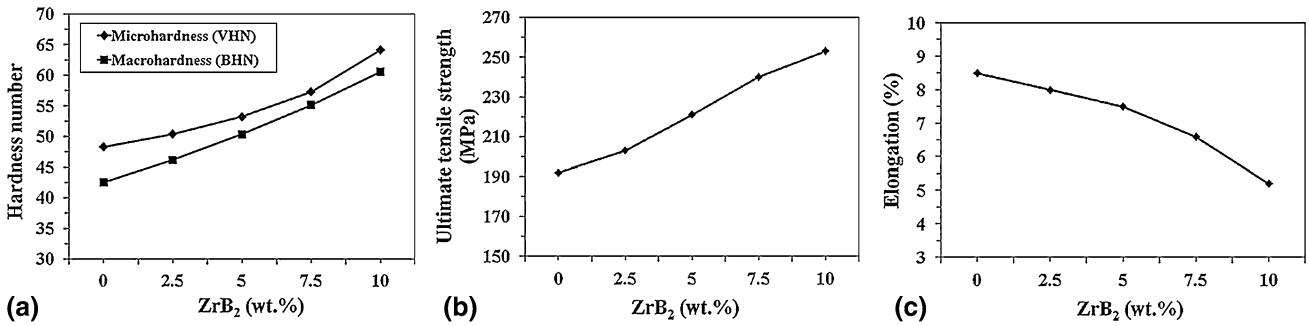

Fig. 14 Hardness, UTS and elongation properties of Al 6061-ZrB_2 composite with increase in wt.% of ZrB_2 (Ref 84)

energy values. The Gibbs free energy values of the following reactions are −860 and −758 kJ/mol, indicating that the reactions are favorable at 727 °C.

$$K_2TiF_6 + 2KBF_4 + 10/3Al \rightarrow TiB_2 + 10/3AlF_3 + 4KF$$

$$K_2ZrF_6 + 2KBF_4 + 10/3Al \rightarrow ZrB_2 + 10/3AlF_3 + 4KF$$

Zhang et al. (Ref 10) have synthesized in situ ZrB_2 and Al_3Zr particles in A356 alloy with the addition of K_2ZrF_6 and KBF_4 salts. The ZrB_2 and Al_3Zr particles are regular hexagon and tetragonal shape with size varying from 0.3 to 0.5 μm with a homogeneous distribution as shown in Fig. 13. The increase in percentage of K_2ZrF_6 and KBF_4 addition resulted in increase in the volume percentage of ZrB_2 and Al_3Zr particles.

The Al-ZrB_2 in situ composites showed improved mechanical and wear properties with the increase in ZrB_2 content. The 6061-10 wt.% ZrB_2 synthesized by the salt reaction method showed a 71% increase in wear resistance, 38% increase in hardness, and 30% increase in UTS, whereas the elongation reduced by 80%, which are shown in Fig. 14 (Ref 84). Tian et al. (Ref 83) reported grain refinement with increase in ZrB_2 content in 2024 Al alloy and observed significant grain refinement with 5.4 wt.% ZrB_2 and no further refinement of grain size achieved when the particle volume fraction is over

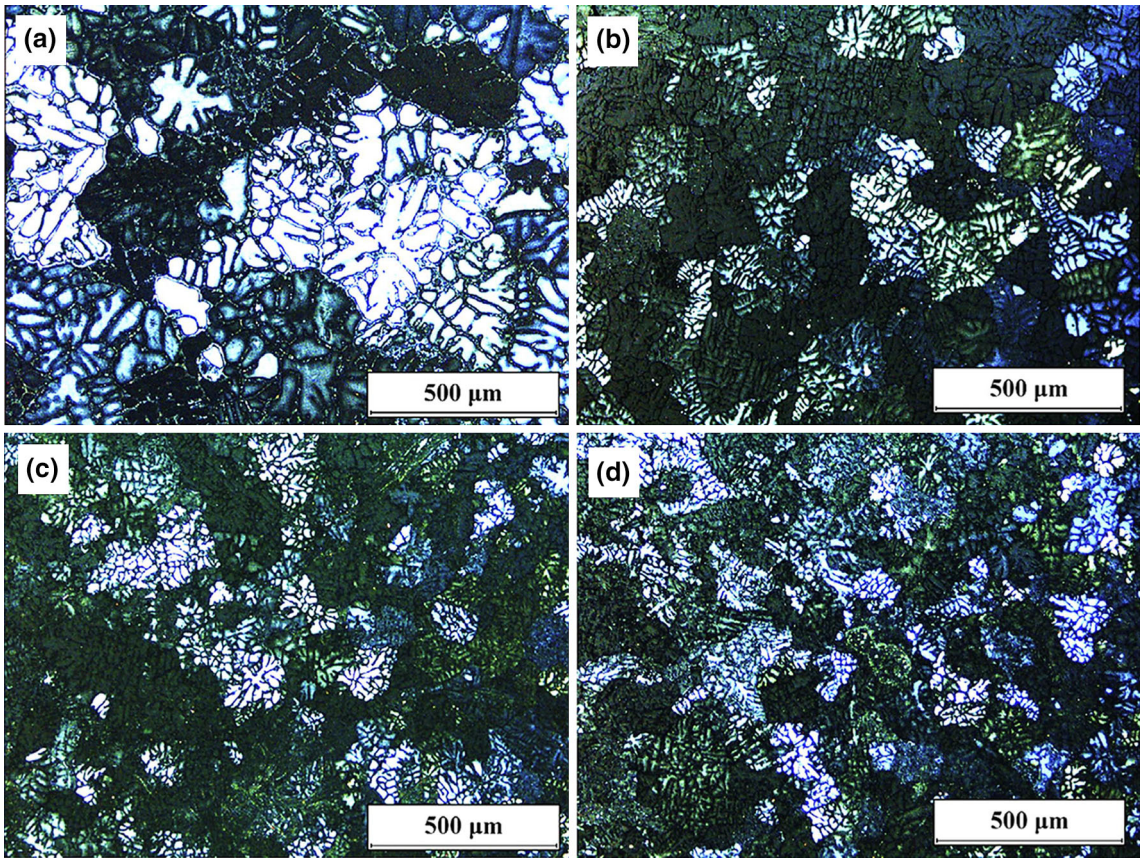

Fig. 15 Optical micrographs of refined specimens with different particle volume fractions. (a) 2024Al alloy, (b) 2024Al-3.1% ZrB_2, (c) 2024Al-5.4% ZrB_2, (d) 2024Al-8.1% ZrB_2 (Ref 83)

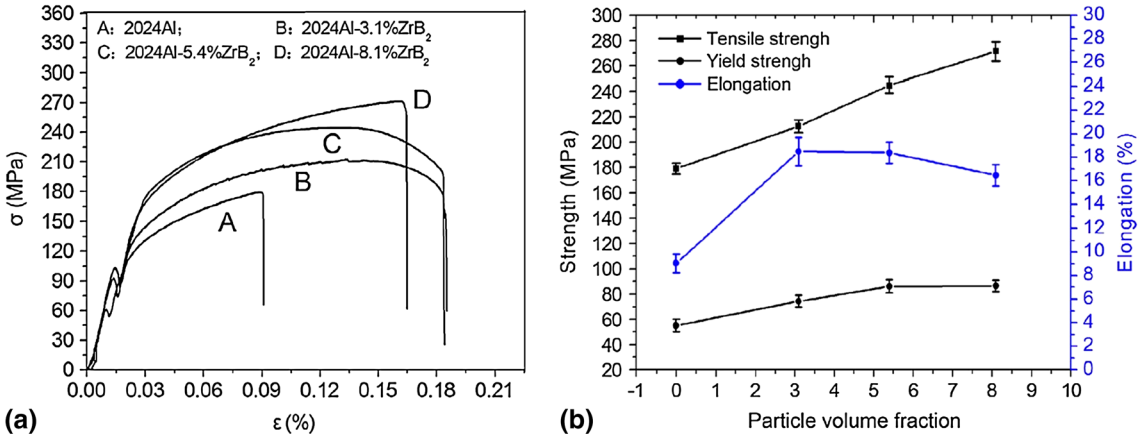

Fig. 16 Tensile strength, yield stress, and elongation of the 2024Al matrix composites reinforced by the ZrB_2nano-particles with different particle volume fractions (Ref 84)

5.4% ZrB_2 which is shown in Fig. 15. The tensile property shows a 50% improvement in tensile strength for 8.5 wt.% ZrB_2 composite compared with 2024 alloy, which is shown in Fig. 16. Wear studies showed better wear resistance with increase in percentage of K_2ZrF_6 and KBF_4 addition. Hardness and wear resistance of the composite shows an increase of 45 and 83% for Al 6351-9 wt.% ZrB_2 composite compared with base Al 6351 alloy. The composite after aging treatment also reported 66% increase in hardness compared with as-cast condition (Ref 86).

1.6 Al-AlN In Situ Composites

Most of the in situ synthesis of Al-AlN composites was processed by the direct reaction of N_2 or NH_3 gas with the molten Al. Zheng et al. (Ref 87) synthesized in situ AlN-

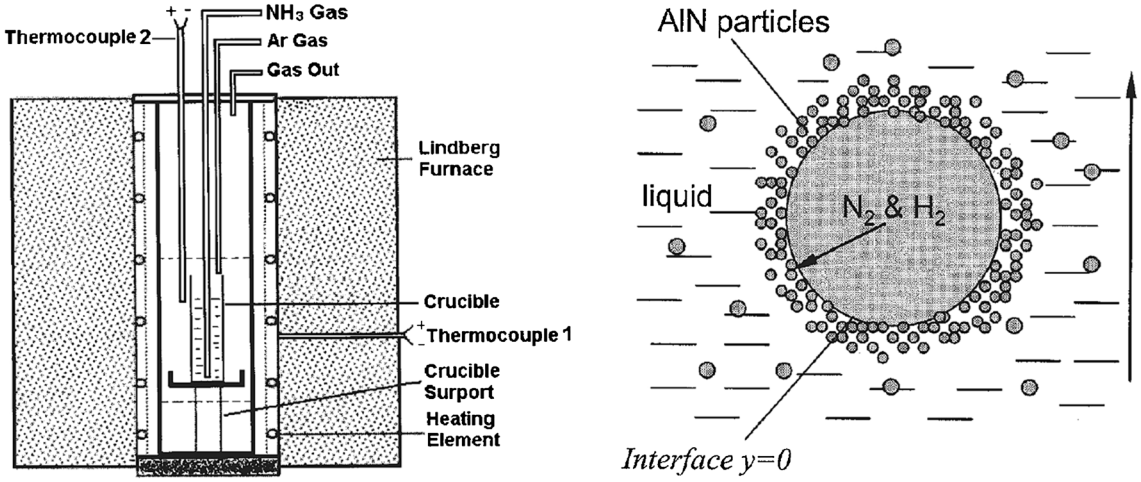

Fig. 17 Schematic of the setup for the AlN formation in Al melt by NH_3 gas purging and model for the formation of NH_3 bubble with Al melt (Ref 87, 88)

reinforced Al matrix composite by bubbling deoxidized N_2 through Al melt and formation of AlN is confirmed by the XRD analysis and particle size of less than 10 μm is reported. Thermodynamics of formation of AlN in Al melt with bubbling of N_2 gas was studied and when commercial N_2 gas was bubbled, significant AlN was not formed because of O_2 content and for significant AlN formation; the O_2 content in the N_2 bubbling gas should be below a critical value. Zheng et al. (Ref 88) also synthesized AlN in situ composites by the addition of NH_3 in to the melt. The mechanism of formation of AlN using ammonia as the bubbling gas was analyzed and optimized with the flow rate and the temperature.

The overall reaction for the formation of AlN is given by

$$2Al\ (l) + 2NH_3(g) \rightarrow 2AlN(s) + 3H_2(g)$$

Ammonia is dissociated into N_2 and H_2 at temperatures above 500 °C. Ammonia is heated in a gas-bubbling tube before entering the matrix melts through the nozzle. The dissociation reaction is given by

$$2NH_3(g) \rightarrow N_2(g) + 3H_2(g)$$

Hence, the AlN reinforcing particles may actually be formed from the reaction between the nitrogen gas and molten aluminum, which is given by

$$2Al(l) + N_2 \rightarrow 2AlN(s)$$

The generated H_2 gas takes away O_2, thereby enhancing the rate of formation of AlN. The Schematic of the processing of Al-AlN composite by NH_3 gas and the mechanism of formation of AlN from the gas bubble was reported by Zheng et al. (Ref 88) and is shown in Fig. 17.

The reaction process for formation of AlN can be described by the two-film model. Various steps in the AlN formation in Al melt are given by Zheng et al. (Ref 87) as (i) mass transfer of N_2 molecules through the gas boundary layer to the gas bubble-Al melt interface, (ii) chemisorption of N_2 molecules at the interface, (iii) mass transfer of the N_2 atoms in the liquid boundary layer (iv) chemical reaction between nitrogen and aluminum atoms to form the AlN particles at the interface, in the liquid boundary layer, and in the bulk matrix melt.

The in situ formation of AlN and TiN in Al-5 wt.% Mg-3wt.% Ti melt was studied by the bubbling of N_2 and 12.5 vol.% NH_3 gas to the melt (Ref 89). The melt was held for 1 h in N_2 atmosphere prior to the bubbling of N_2-NH_3 mixture to avoid O_2 content in the melt. XRD analysis showed AlN, TiN, and Al_3Ti peaks and the AlN and TiN particles were observed to move to the top of the crucible along with the gas. Al-AlN in situ composite was synthesized by Kumari et al. (Ref 90) by N_2 purging in Al melt and reported the morphology of particles to be hexagonal with a particle size ranging from nano, submicron to a few microns. The optical micrographs of in situ Al-AlN after 2 h of reaction and Al-4Mg-AlN composite after 4 h of reaction at gas flow rate of 0.4 lpm is shown in Fig. 18. The AlN formation is confirmed by the XRD analysis of the extracted particles. Presence of Mg in the melt enhances the reaction rate, and net-work of interconnected AlN particles are formed. The Mg is expected to react with O_2 to form MgO and enhance AlN formation.

Fale et al. (Ref 91) studied the formation of Al-AlN in situ composite by the addition of NH_4Cl and CaO as nitriding precursers in Al melt. The NH_4Cl and CaO are added to molten Al at three different temperatures 700, 800, and 900 °C. NH_4Cl reacts with CaO to form NH_3 which dissociates into nascent nitrogen at higher temperature and reacts with Al melt to form AlN. Initiation of heterogeneous nucleation requires sites like surfaces and interfaces and in this case the heterogeneous nucleation site is between nascent nitrogen gas bubbles and the melt. The bubbles generated at higher temperature are big and the particle size is also large. Increase in processing temperature increases the particle size as well as the agglomerate size. At lower temperature, the wetting angle of the AlN particle with Al is higher and particle size is also less. Thermodynamic calculations were carried out by Fale et al. (Ref 91) and the critical radius of nuclei and ΔG_{hetro} was found to increase with increase in temperature.

Wang et al. (Ref 92) synthesized Al-AlN in situin situ composites by passing plasma jet in to Al-5Ti-B alloy. The Plasma gas (Ar + N_2) was injected in to the melt and in situ AlN and TiN particles form in aluminum matrix along with TiB_2, Al_3Ti, and Al_2O_3. AlN is formed due to the direct reaction of N_2 with Al and TiN forms by the reaction of Ti from the decomposition of Al_3Ti with N_2. With the increase in nitriding time, the volume percentage of the particles increases

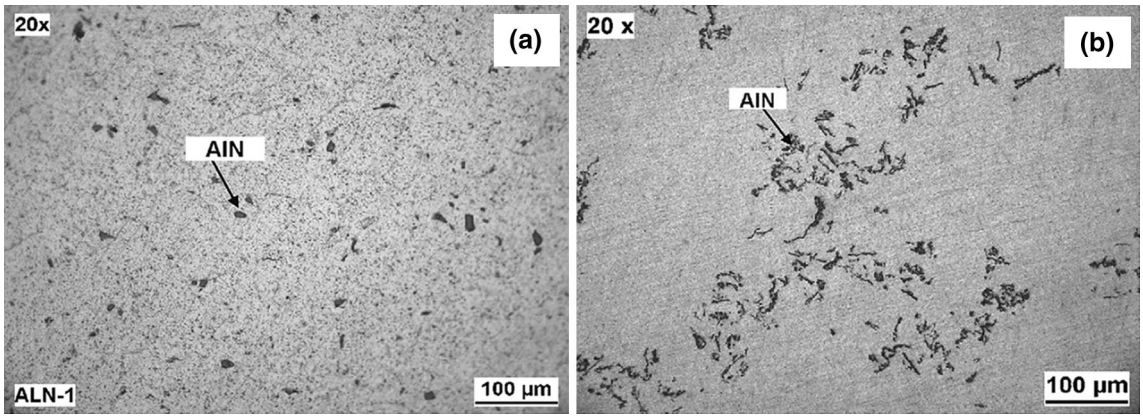

Fig. 18 The optical micrographs of (a) in situ Al-AlN after 2 h reaction and (b) Al-4Mg-AlN composite after 4 h reaction at gas flow rate of 0.4 lpm (Ref 90)

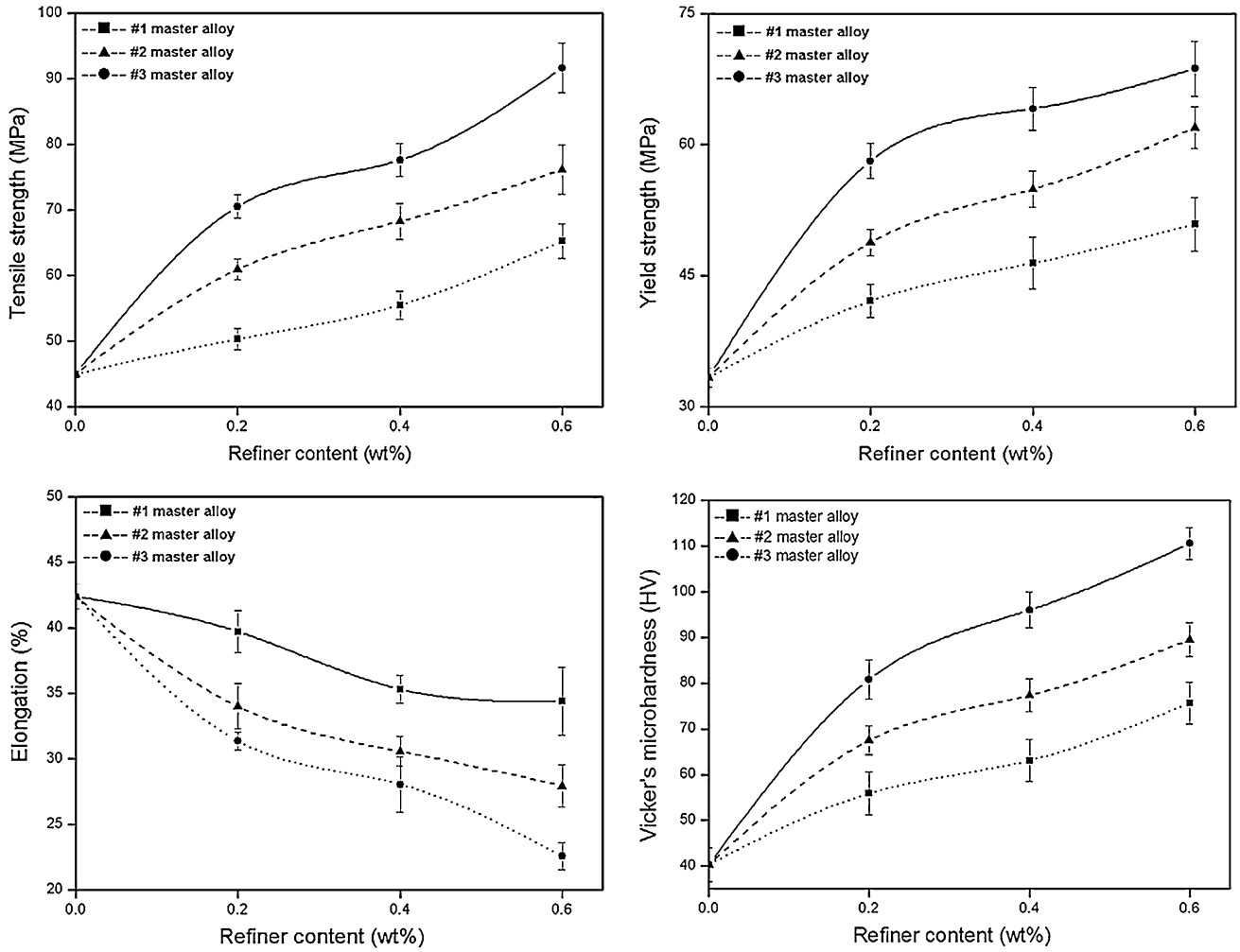

Fig. 19 The mechanical properties of Al-AlN/TiN composite with various reinforcement contents in three alloys prepared with 10, 20, and 30 S nitriding time (Ref 92)

and hence the nucleating sites increases, thus reducing the grain size and increasing the mechanical properties.

Al-AlN in situ composites showed an increase in mechanical properties with the increase in fraction of the reinforcement. Sandeep et al. (Ref 2) studied the wear behavior of Al-AlN in situ composite and with the good dispersion and higher weight fraction of AlN particles showed better wear resistance under dry sliding condition. Kumariet al. (Ref 90)

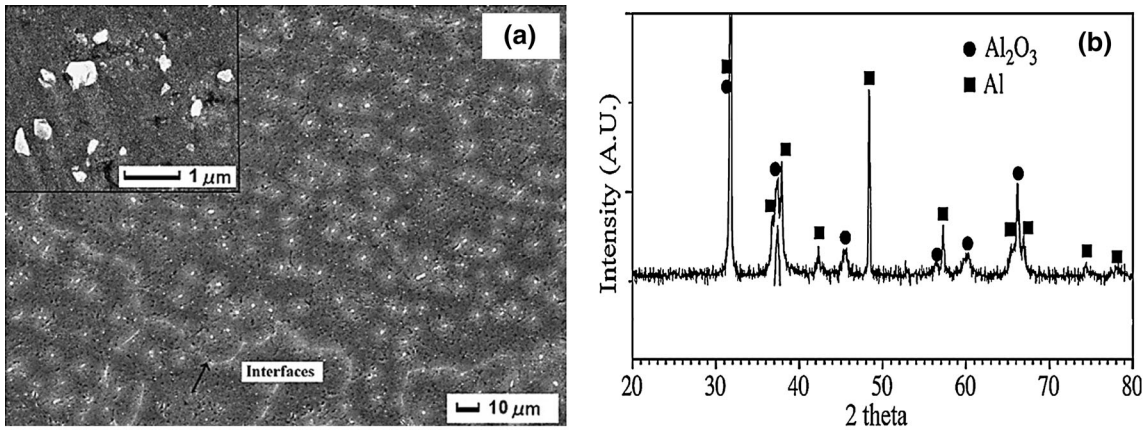

Fig. 20 (a) SEM micrograph of cast Al-Al_2O_3 composite showed uniform distribution of the particle and (b) XRD graph of the composite shows the formation of Al_2O_3 (Ref 6)

reported improvement in hardness with the AlN reinforcement. Al-AlN in situ composites prepared by injecting plasma jet in to Al-5Ti-B alloy show an increase in UTS and tensile strength in the order of 2 with 0.6 wt.% of AlN and TiN reinforcement in Al alloy (Ref 92). The tensile strength, yield strength, Elongation, and hardness values are plotted with the increase in AlN and TiN reinforcement content and are shown in Fig. 19. It can be observed that, with increase in wt.% of the reinforcement, tensile strength, yield strength, and hardness increases and elongation are reduced.

1.7 Al-Al_2O_3 In Situ Composites

There are various methods to synthesize Al-Al_2O_3 in situ composites, the most popular being directed melt oxidation (DIMOX) of aluminum alloys, in which the melt is held at higher temperature with oxide forming solute elements or other oxides (Ref 6, 93-99). Other method is directly passing O_2 in to the Al melt (Ref 100) so that it can react and form Al_2O_3 inside the Al melt. Commonly used in situ processing of Aluminum composites with Al_2O_3 reinforcement is by the reaction between metal oxide and Al melt. Most of the Al-Al_2O_3 composites are synthesized by DIMOX of aluminum alloys. The in situ processing of Al_2O_3 in Al melt was by the reaction of a molten alloy with a gaseous oxidant. The DIMOX process was developed by Lanxide Corporation, USA to process Aluminum matrix composites. Various solute elements like Mg, Zn, Li, and other oxygen carrying solute elements are added to obtain continuous thermal oxidation of the alloy. Murthy et al. (Ref 99) studied the directed melt oxidation of AI-Mg-Si alloys. In case of Al alloys containing Mg, first Mg oxidises and forms MgO layer on the top of the melt and MgO further reacts with aluminum to form $MgA1_2O_4$ when the melt is held above liquidus temperature. The oxide layer is in contact with the liquid metal beneath. The micro-cracks or porosity in the oxide layers give way to the liquid alloy and the liquid emerges to the top and forms droplets and later forms oxidation front. The formation of $A1/Al_2O_3$ composite structure begins when the magnesium concentration reaches the equilibrium phase field $MgA1_2O_4$ + $A1_2O_3$ + liquid alloy (Mg, A1). In situ synthesis of Al_2O_3 in Al alloys can also be done by direct purging of O_2 to the alloy melt without any oxide enhancers other than the alloying elements. In situ Al_2O_3 particle reinforced LM24 alloy was synthesized by direct reaction between oxygen and Al melt at 750-800 °C by passing O_2 through Fe tube with insulation into the melt directly (Ref 100).

In situ synthesis of Al_2O_3 in Al alloys was obtained by the reaction of combination of oxides or oxide with the Al melt at 850-900 °C temperature. Al-Al_2O_3 in situ composites can also synthesized by the reaction of CuO (Ref 96) and Fe_2O_3 (Ref 97) particles in molten Al. In case of CuO addition, the CuO particles reacted with molten Al to form Al_2O_3 and pure Cu particles. In case of Fe_2O_3 additions, thermodynamic calculations were done and find the reaction temperature of 700 °C for the Fe_2O_3 particles and Al reaction. Fe_2O_3 particles were added to produce 1.3 wt.% Al_2O_3 and Al_2O_3 particles are reported to be round shaped and are of 0.5-1 μm.

Hoseini et al. (Ref 95) synthesized in situ Al-Al_2O_3 composite by the reaction of glass powder (amorphous SiO_2) and CuO with the Al melt. CuO prevents the sticking of SiO_2 and act as reduction reaction starter. A typical reduction reaction of a metallic oxide in an aluminum melt was given by

$$3MeO + 2Al \rightarrow Al_2O_3 + 3Me$$

The reaction for CuO and SiO_2 with Al is give by

$$3CuO + 2Al \rightarrow Al_2O_3 + 3Cu,$$
$$\Delta G^\circ = -1190 - 0.034T \text{ (kJ/mole } Al_2O_3)$$

$$1.5SiO_2 + 2Al \rightarrow Al_2O_3 + 1.5Si,$$
$$\Delta G^\circ = -310.7 - 0.04T \text{ (kJ/mole } Al_2O_3)$$

Thermodynamically, according to the above reaction, Al reduces silicon oxide (glass powder) and produces Si and Al_2O_3. Also CuO will react with molten Al and forms Al_2O_3. 38% improvement in UTS and 70% improvement in hardness compared with pure Al was obtained with the addition of 2 wt.% CuO. The improvement in the mechanical properties is from the solid solution strengthening of Cu solute and particulate strengthening of Al_2O_3.

Wang et al. (Ref 93) synthesized Al-Al_2O_3 in situ composites via direct melt reaction by adding $Ce_2(CO_3)_3{\cdot}nH_2O$ powder and studied thermodynamics of in situ chemical reaction between molten Al and CeO_3. $Ce_2(CO_3)_3$ decomposes as CeO_2 and CO_2 when it is preheated at 200-300 °C in the drying oven without any protective atmosphere. The reactions of $Ce_2(CO_3)_3$decomposition at 200-300 °C, reaction of CeO_2 with Al and formula for Gibbs free energy of CeO_2 and Al_2O_3 are shown below.

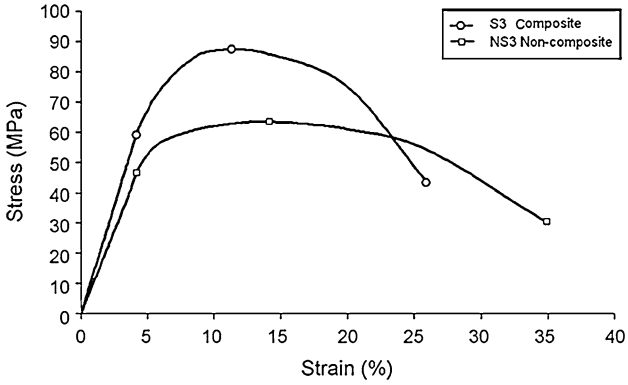

Fig. 21 Stress-strain curve for composite and non-composite specimens at 300 °C (Ref 95)

$$Ce_2(CO_3)_3 \rightarrow CeO_2 + CO_2 \uparrow (200-300^{\circ}C)$$

$$4Al + 3CeO_2 \rightarrow 2Al_2O_3 + 3Ce(800-900^{\circ}C)$$

$$\Delta G^{\circ}CeO_2 = -1029,260 + 214.22T \quad (J/mol\,O_2)$$

$$\Delta G^{\circ}Al_2O_3 = -1120,480 + 214.22T \quad (J/mol\,O_2).$$

At standard condition (*o*), the Gibbs free energy of reaction is calculated as −91.2 kJ/mol O_2 (that is $\Delta G^{\circ}Al_2O_3 - \Delta G^{\circ}CeO_2$). The entropy values of CeO_2 and Al_2O_3 are nearly equal. So the reaction between aluminum and CeO_2 components has little relevance to the reaction temperature. The reaction between aluminum and cerium oxide can proceed spontaneously and the melt temperature is determined as 850 °C. The formation of Al_2O_3 is confirmed by the XRD analysis of Al-Al_2O_3 composite (Fig. 20). The Al_2O_3 particle size formed is of 100-200 nm with uniform distribution and is shown in Fig. 20.

Yang et al. (Ref 94) synthesized Al-Al_2O_3 composites by displacement reaction of CuO, SiO_2, and MnO_2 powders in which the powders were added as preforms with proper ratios of Al and CuO, or Al, CuO, and SiO_2, or Al, CuO, SiO_2, and MnO_2 into the molten aluminum at 900 °C to produce the Al-Cu-Al_2O_3, Al-Si-Cu-Al_2O_3, Al-Si-Cu-Mn-Al_2O_3 composites.

Al-Al_2O_3 composite synthesized by SiOand CuO addition shows an increase of 40% in the high-temperature tensile strength at 300 °C in comparison with the base Al, and the stress strain curve is shown in Fig. 21. The alloy showed low strain hardening at high temperatures, observed from the tensile curve, which is almost parallel to the strain axis. The composite shows higher strain hardening. LM24-Al_2O_3 composite showed 30% improvement in yield strength and 10% increase in UTS compare with LM24 alloy (Ref 100). Al-Al_2O_3 composite shows 30% improvement in UTS for 4.24 wt.% Al_2O_3 composite at 300 °C compare with base alloy (Ref 97).

1.8 Al-Mg_2Si In Situ Composites

Mg_2Si reinforcement in Al is synthesized during the solidification of Al alloy containing Si and Mg. The Al-Si-Mg system forms blocky-type primary Mg_2Si and flat-like morphology eutectic or pseudo-eutectic Mg_2Si inside the eutectic cell. Several investigations were carried out by researchers to modify the primary and eutectic Mg_2Si phase (Ref 101-106). To modify the primary Mg_2Si and flat-like morphology eutectic or pseudo-eutectic Mg_2Si phase, various elements, Sb, Pb, Na, Y, Sr, Na or compounds, K_2TiF_6, were added. Y addition changes the pseudo-eutectic morphology from flate-like to fibrous (Ref 104). Sb and Li addition changes the primary Mg_2Si morphology (Ref 102, 103). K_2TiF_6 addition changes the primary and eutectic Mg_2Si morphology (Ref 107). Mg_2Si is having anti-fluorite structure with FCC crystal symmetry and 12 atoms in the unit cell with Si atoms at corners and face-centered positions and eight Mg atoms forming a cubic sub-lattice inside the unit cell (Ref 108). Al-15 wt.% Mg_2Si particles were produced in situ during the solidification process of Al-Si-Mg alloy at 800 °C (Ref 14). According to the binary phase diagram of Al-Mg_2Si system, the composition of the Al-15% Mg_2Si composite is in hypereutectic region and the as-cast microstructure consists of primary Mg_2Si and pseudo-eutectic structure. Primary Mg_2Si particle was refined and spherical α-Al grains were produced by addition of extra Si in the composites. Irregular-shaped primary Mg_2Si particles with a mean size of about 30 μm were obtained.

Al-Mg_2Si forms a pseudo-eutectic system in Al-Mg-Si system. The change in morphology of irregular to polyhedral with the addition of NaCl, NaF, and KCl salts (Ref 109). The Mg_2Si phase formed during the in situin situ processing of Al-Si-Mg alloy is usually coarse and ultrasonic vibration was used by Ko et al. (Ref 101) to refine the Mg_2Si particle and average size of primary Mg_2Si was reduced from 70 to 15 μm; morphology was also changed to polygonal from irregular shape, which is shown in Fig. 22. Zhang et al. (Ref 110) also studied the effect of ultrasonic vibration in the Mg_2Si morphology and the mean grain size of primary Mg_2Si crystals is refined from 150 to 20 μm by high intensity ultrasonic vibration, and the morphologies of primary Mg_2Si crystals are changed as well. Mg_2Si in situ reinforcement was synthesized by the addition of Mg in to Al-12Si alloy (Ref 111). The volume fraction and size of the primary Mg_2Si particles increased with increasing the Mg content. Observed two different morphologies of Mg_2Si polyhedral primary particle and as a chinese script morphology. Mandal et al. (Ref 1) studied the effect of high Mg in Al-7Si alloy in which the microstructure showed spheroidal Mg_2Si and eutectic Si particles dispersed in α-Al. With high Mg, and combination of Sr addition followed by T6 treatment resulted in a fine and spheroidal eutectic mixture of Si and Mg_2Si. Increase in Mg content increase the Mg_2Si content and thereby increases the hardness.

Emamy et al. (Ref 112) studied the effect of Na on the microstructure and Na restrict the growth of Mg_2Si by poisoning growth sites on the surface of the Mg_2Si nuclei and create some distortion in the Mg_2Si lattice and thus change the surface energy of the Mg_2Si. Average particle size decreases from 32 to 7 μm with the addition of 0.1 wt.% Na which is shown in the Fig. 23. The volume fraction of α-Al in pseudo-eutectic matrix increases by the addition of Na up to 0.15%. Also study the effect of yttrium addition on Mg_2Si phase (Ref 104) and Y addition does not change the size and morphology of primary Mg_2Si particles considerably, but the pseudo-eutectic Mg_2Si was changed from a flake-like morphology to fine fibrous or rod-like. The addition of 2 wt.% Fe to the Al-15 wt.% Mg_2Si composite changes the morphology of primary

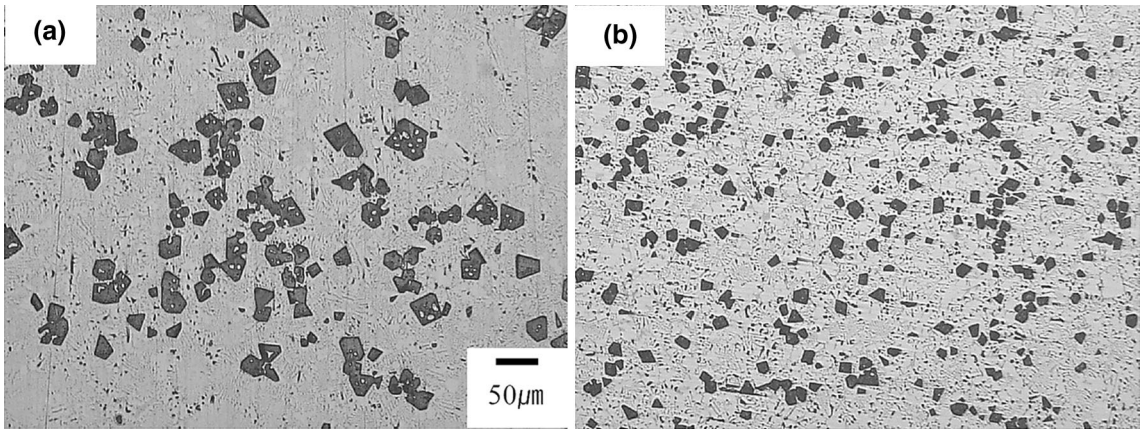

Fig. 22 Optical micrograph of Al-12Mg-6.9Si alloy (a) without ultrasonic injection (b) with ultrasonic injection (Ref 102)

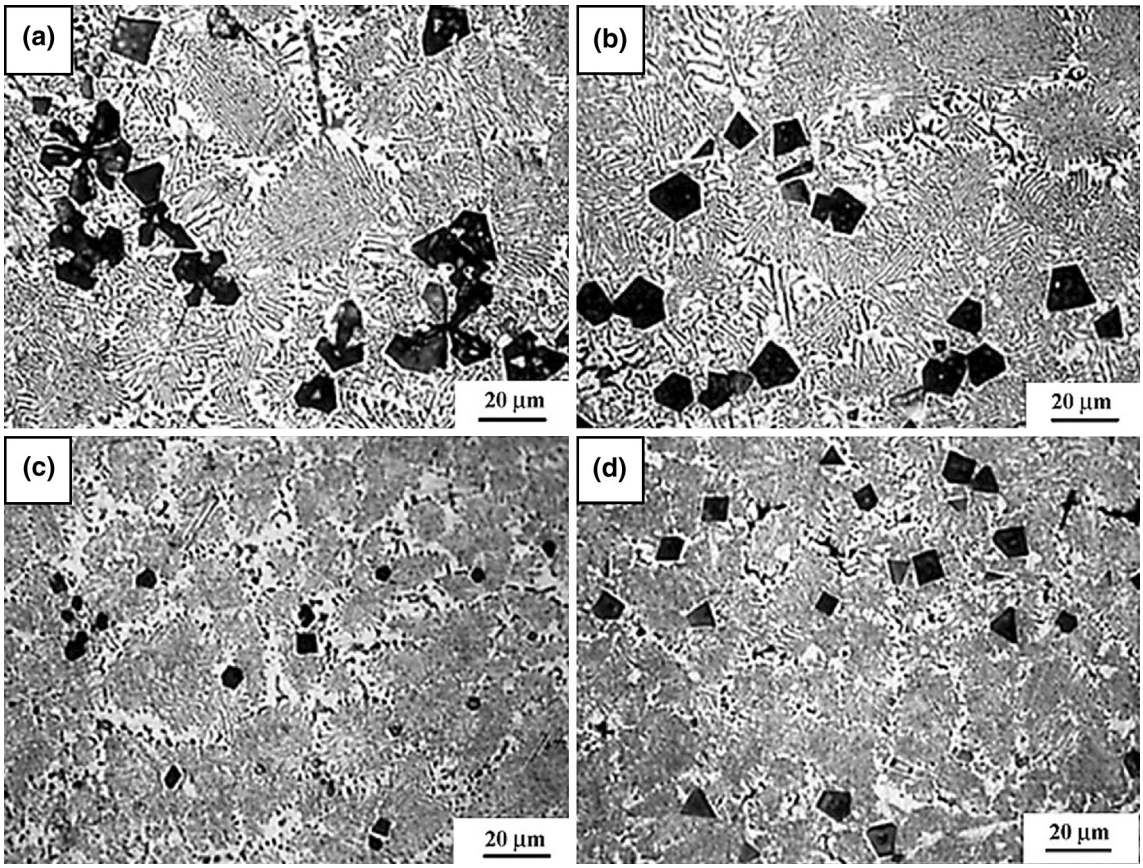

Fig. 23 Optical microstructures of in situ Al-15 wt.%Mg_2Si composite with different Na additions. (a) 0 wt.%, (b) 0.05 wt.%, (c) 0.1 wt.% and (d) 0.15 wt.% (Ref 112)

Mg_2Si from irregular to polyhedral shape and reduces its average particle size from 33 to 15 μm (Ref 113).

Al-Si-11Mg_2Si in situ composite was prepared by a modified investment casting technique (Ref 114). The as-cast composite consists of primary α-Al dendrites enveloped in a layer comprising crystallites of pre-eutectic Mg_2Si within primary Al. The dendrite boundaries are surrounded by the pseudo-eutectic micro-constituent Al-Mg_2Si, where the Mg_2Si precipitates have the morphology of Chinese script. Spheroidization of the primary precipitates was obtained by solution treatment at 540 °C. Malekan et al. (Ref 115) also studied the solutionizing effect on microstructure and found out that not only the size of primary Mg_2Si phase changes but the eutectic Mg_2Si phase also changes to fine dot-like morphology.

Al-15 wt.% Mg_2Si metal matrix composite was processed and study the effect of Li addition on modification of Mg_2Si phase (Ref 102) and 0.3% Li addition results in reduction of average size of Mg_2Si primary particles from 30 to 6 μm,

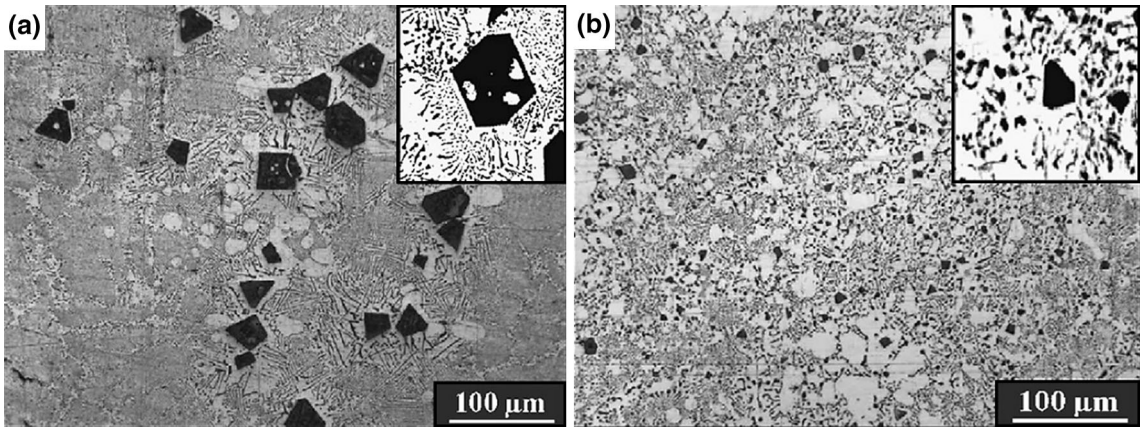

Fig. 24 Microstructure of permanent mold Al-15%Mg_2Si composite and (b) the microstructure after modification with 0.3%Li (Ref 102)

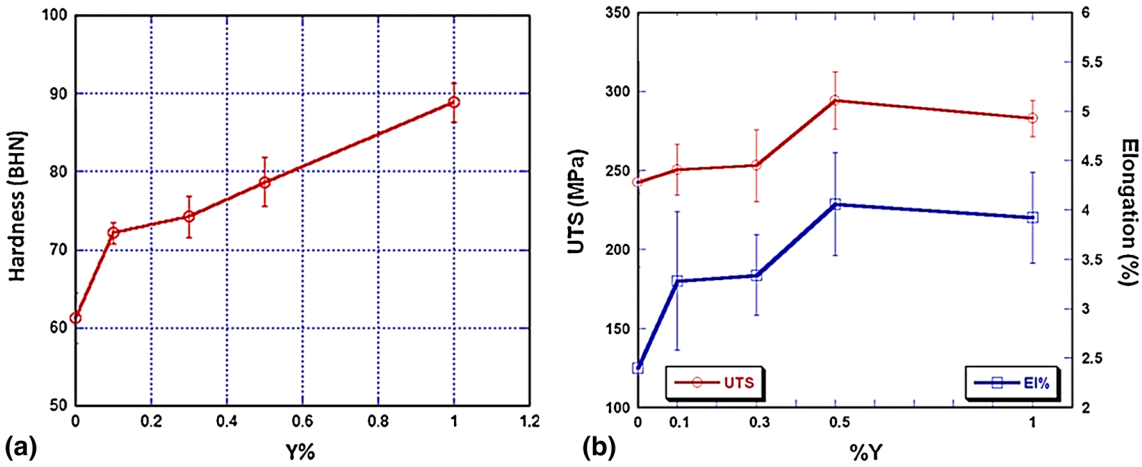

Fig. 25 (a) Hardness of Al-15%Mg_2Si composite and (b) UTS and Elongation as a function of Y concentration (Ref 104)

which is shown in Fig. 24. Sun et al. (Ref 116) studied the effect of 0.05% Sr, 0.20% of red phosphorous and 0.30% of NaCl + 30 $MgCl_2$ + 10 KCl mixtures in Al-12Si with 5-20% Mg reinforced Mg_2Si composite and observed increase in volume fraction and size of the primary Mg_2Si particle. 0.4% Sb addition in Al-Si alloy reinforced with in situ Mg_2Si composite refines the primary Mg_2Si phase (Ref 103). Primary Mg_2Si particle morphology is changed from dendritic to polygonal, and its size decreases from 47.5 to 13.0 μm with the addition of Nd in Al-18 wt.% Mg_2Si in situ composites. Also, the morphology of the eutectic Mg_2Si phase is altered from flake-like to a thin laminar, short fibrous, and coral-like or dot-like structure (Ref 3).

Lin et al. (Ref 117) fabricated Al-Mg_2Si FGM tube by centrifugal casting. Many primary Si and Mg_2Si particles existed in the inner layer of the tube due to the lower density and effect of centrifugal force. The particle size of primary Si and primary Mg_2Si showed an obviously graded distribution in the reinforcement layer of the FGMs fabricated with high pouring or mold temperatures and their diameters changed from 70 to 30 μm and from 30 to 18 μm, respectively.

The effect of mechanical and wear behavior of in situ Mg_2Si composites was reported by many researchers. The modification of primary and eutectic Mg_2Si particle further improves the mechanical and wear properties (Ref 105-107, 109, 110, 115, 118, 120). Li addition in Al-15 wt.% Mg_2Si composite reduces the size of primary Mg_2Si and improved elongation in order of two and 20% improvement in UTS (Ref 119). With the effect of ultrasonic vibration in the Al-Mg_2Si composite melt, the Mg_2Si particle size got refined and the tensile strength was improved by 30%, from 112 to 148 MPa, which is shown in Fig. 25 (Ref 101). Ahlatci et al. (Ref 111) and Sun et al. (Ref 116) reported 1.5 times improvement in the hardness and 40% improvement in compressive strength with the addition of 20% Mg in Al-12Si alloy (Al-5Si-45V_f Mg_2Si in final composition). Na addition refines the size of primary Mg_2Si particles in Al-15 wt.% Mg_2Si composite and with 0.1 wt.% Na addition, 12% improvement in UTS and 38% improvement in percentage elongation obtained (Ref 112).

The large and brittle Mg_2Si particles may act as crack initiators, while fine rod-like morphology of eutectic Mg_2Si in Al-Mg_2Si composite with 0.5 *Y* addition acts as barrier to the

propagation of cracks and thus enhance the elongation values. Emamy et al. (Ref 1) reported a 33, 60, and 12% increase in hardness, percentage elongation, and UTS, respectively, with *Y* addition as shown in Fig. 25. At higher *Y* contents, an intermetallic phase (Al_2Y), introduced on eutectic cell boundaries, appears to be the favored path for crack propagation (Ref 104). Effect of heat treatment on tensile properties of Na-modified Al-Mg_2Si in situ composite shows an increase in the elongation values and the UTS reduces (Ref 105). Malekan et al. (Ref 115) also studied the effect of solutionizing and reported decrease in UTS with increase in solutionizing temperature, whereas the elongation increases till 500 °C and then reduced at temperatures of 550 and 580 °C. Fe addition improves hardness by changing the morphology of primary Mg_2Si particle and formation of Fe-based intermetallic, while the Fe containing samples shows brittle fracture. 3.5 wt.% Fe in Al-Mg_2Si die-cast composite shows an increase of 50% in hardness, 20% increase in UTS, no significant change in yield strength and reduction in elongation by the order of two (Ref 113). Georgatis et al. (Ref 114) also reported a decrease in tensile property with the presence of Fe content.

Effect of Ti on extruded in situ Al-15% Mg_2Si composite showed 40% improvement in UTS and elongation also showed transition from brittle fracture mode in the as-cast composite to ductile fracture extruded specimens (Ref 120). Soltani et al. (Ref 9) also studied the effect of hot extrusion on wear properties of Al-15 wt.% Mg_2Si in situ metal matrix composites and showed an improvement in wear resistance for higher extrution ratio samples and observed abrasion to be the dominant wear mechanism in all extruded composites, whereas combination of adhesion and delamination appears to be the governing mechanism for as-cast composites.

The wear behavior is found to improve by the addition of Sb in Al-Mg_2Si composites. Sb addition refines the primary Mg_2Si particles and during wear, the Mg_2Si granules slide between wearing surface as hard particles, which shear, pear crease, and cut wearing surface and the main wear mechanism is grain-abrasion (Ref 103). The addition of Nd also changes the wear mechanism of the composite from the combination of abrasive, delamination, and adhesive wear without Nd to mild abrasion and adhesive wear with 0.1 wt.% Nd and then to a single mild abrasion wear with 0.5 wt.% Nd. The low wear rate for the composites with Nd is mainly due to the size refinement and morphology change of primary and eutectic Mg_2Si (Ref 3). 0.5 wt.% Nd addition in Al-18 wt.% Mg_2Si in situ composite showed a 32.4% increase in UTS and 200% increase in percentage elongation also Nd addition changed the fracture behavior from brittle to ductile (Ref 121).

2. Conclusions

Al-based in situ cast composites with various reinforcements and their processing methods are summarized. The influence of various process parameters on the nature, size, and morphology of reinforcement particles is discussed in detail. Many of these in situ composites show excellent mechanical and wear properties with increase in reinforcement content. The tensile and yield strength show significant increase but the ductility appears to reduce with the increase in reinforcement fraction. Reinforcement particles in sub-micron sizes appear to demonstrate a good combination of strength and ductility in these in situ composites. The influence of secondary mechanical processing after the synthesis of cast composites to improve the particle distribution and strength is also highlighted. Heat treatment also is found to be good for improving the properties of composites. TiB_2 and Mg_2Si reinforcements attracted the attention of most of the researchers because of their easiness to fabricate and cost effectiveness. Since primary Mg_2Si phase is coarse, efforts have been made to refine the Mg_2Si particle to improve the mechanical properties. TiB_2, TiC, and ZrB_2 particles, in addition to acting as reinforcements, also lead to grain refinement of the Al matrix as they are good nucleating sites for Al.

References

1. A. Mandal, N. Chippa, K. Jayasankar, and P.S. Mukherjee, Effect of High Magnesium Content on Microstructure of Al-7Si Alloy, *Mater. Lett.*, 2014, **117**, p 168–170
2. S. Fale, A. Likhite, and J. Bhatt, The Wear Behavior of In situ Al-AlN Metal Matrix Composites, *Trans. Indian Inst. Met.*, 2014, **67**, p 841–849
3. X. Wu and G. Zhang, Microstructure and Dry Sliding Wear Behavior of Cast Al-Mg_2Si In-Situ Metal Matrix Composite Modified by Nd, *Rare Met.*, 2013, **32**, p 284–289
4. C.J. Song, Z.M. Xu, G. Liang, and J.G. Li, Study of In-Situ Al/Mg_2Si Functionally Graded Materials by Electromagnetic Separation Method, *Mater. Sci. Eng. A*, 2006, **424**, p 6–16
5. P. Li, E.G. Kandalova, and V.I. Nikitin, In Situ Synthesis of Al-TiC in Aluminum Melt, *Mater. Lett.*, 2005, **59**, p 2545–2548
6. H. Wang, G. Li, Y. Zhao, and G. Chen, In Situ Fabrication and Microstructure of Al_2O_3 Particles Reinforced Aluminum Matrix Composites, *Mater. Sci. Eng. A*, 2010, **527**, p 2881–2885
7. M.F. Najafabadi, M.A. Golozar, A. Saidi, and H. Edris, Wear Behaviour of Aluminium Matrix TiB_2 Composite Prepared by In Situ Processing, *Mater. Sci. Technol.*, 2014, **19**, p 1531–1532
8. K. Niranjan and P.R. Lakshminarayanan, Dry Sliding Wear Behaviour of In Situ Al-TiB_2 Composites, *Mater. Des.*, 2013, **47**, p 167–173
9. N. Soltani, H.R.J. Nodooshan, A. Bahrami, M.I. Pech-canul, W. Liu, and G. Wu, Effect of Hot Extrusion on Wear Properties of Al-15 wt.% Mg_2Si In Situ Metal Matrix Composites, *Mater. Des.*, 2014, **53**, p 774–781
10. S. Zhang, Y. Zhao, G. Chen, X. Cheng, and X. Huo, Fabrication and Dry Sliding Wear Behavior of In Situ Al-K $_2ZrF_6$-KBF_4 Composites Reinforced by Al_3Zr and ZrB_2 Particles, *J. Alloys Compd.*, 2008, **450**, p 185–192
11. S. Kumar, V. Subramanya Sarma, and B.S. Murty, Effect of Temperature on the Wear Behavior of Al-7Si-TiB_2 In-Situ Composites, *Metall. Mater. Trans. A*, 2008, **40**, p 223–231
12. A. Mandal, B.S. Murty, and M. Chakraborty, Sliding Wear Behaviour of T6 Treated A356-TiB_2 In-Situ Composites, *Wear*, 2009, **266**, p 865–872
13. A. Mandal, M. Chakraborty, and B.S. Murty, Effect of TiB_2 Particles on Sliding Wear Behaviour of Al-4Cu Alloy, *Wear*, 2007, **262**, p 160–166
14. J. Zhang, Z. Fan, Y. Wang, and B. Zhou, Microstructure and Mechanical Properties of In Situ Al-Mg_2Si Composites, *Scripta Mater.*, 2000, **16**, p 913–918
15. B. Basu and K. Balani, *Advanced Structural Ceramics*, Wiley, New York, 2011, ISBN 978-1-118-03729-4
16. C. Barry Carter and M. Grant Norton, *Ceramic Materials*, Springer, New York, 2013, ISBN 978-1-4614-3523-5
17. P. Davies, J.L.F. Kellie, D.P. Parton, London and Scandinavian, Co. Ld., Patent, 1993, WO 93/05189
18. A. Mandal, M. Chakraborty, and B.S. Murty, Ageing Behaviour of A356 Alloy Reinforced with In-Situ Formed TiB_2 Particles, *Mater. Sci. Eng. A*, 2008, **489**, p 220–226
19. S. Lakshmi, L. Lu, and M. Gupta, In Situ Preparation of TiB_2 Reinforced Al Based Composites, *J. Mater. Pro. Tech.*, 1997, **73**, p 160–166

20. S. Kumar, M. Chakraborty, V. Subramanya Sarma, and B.S. Murty, Tensile and Wear Behaviour of In Situ Al-7Si/TiB_2 Particulate Composites, *Wear*, 2008, **265**, p 134–142
21. N. Charbhai, B.S. Murty, and S. Sankaran, Characterization of Microstructure and Precipitation Behavior in Al-4Cu-*x*TiB_2 In-Situ Composite, *Trans. Indian Inst. Met.*, 2011, **64**, p 117–121
22. S.H. Nandam, S. Sankaran, and B.S. Murty, Precipitation Kinetics in Al-Si-Mg/TiB_2 In-Situ Composites, *Trans. Indian Inst. Met.*, 2011, **64**, p 123–126
23. G.S. Vinod Kumar, B.S. Murty, and M. Chakraborty, Development of Al-Ti-C Grain Refiners and Study of Their Grain Refining Efficiency on Al and Al-7Si Alloy, *J. Alloys Compd.*, 2005, **396**, p 143–150
24. S. Kumar, V.S. Sarma, and B.S. Murty, Influence of In Situ Formed TiB_2 Particles on the Abrasive Wear Behaviour of Al-4Cu Alloy, *Mater. Sci. Eng. A*, 2007, **465**, p 160–164
25. S. Kumar, V. Subramanya Sarma, and B.S. Murty, A Statistical Analysis on Erosion Wear Behaviour of A356 Alloy Reinforced with In Situ Formed TiB_2 Particles, *Mater. Sci. Eng. A*, 2008, **476**, p 333–340
26. K.R. Ravi, M. Saravanan, R.M. Pillai, A. Mandal, B.S. Murty, M. Chakraborty, and B.C. Pai, Equal Channel Angular Pressing of Al-5 wt.%TiB_2 In Situ Composite, *J. Alloys Compd.*, 2008, **459**, p 239–243
27. S. Kumar, V. Subramaniya Sarma, and B.S. Murty, Functionally Graded Al Alloy Matrix In-Situ Composites, *Metall. Mater. Trans. A*, 2009, **41**, p 242–254
28. S. Kumar, V. Subramaniya Sarma, and B.S. Murty, The Influence of Room Temperature and Cryogenic Temperature Rolling on the Aging and Wear Behaviour of Al-4Cu-5TiB_2 In Situ Composites, *J. Alloys Compd.*, 2009, **479**, p 268–273
29. A. Mandal, B.S. Murty, and M. Chakraborty, Wear Behaviour of Near Eutectic Al-Si Alloy Reinforced with In-Situ TiB_2 Particles, *Mater. Sci. Eng. A*, 2009, **506**, p 27–33
30. S. Kumar, V.S. Sarma, and B.S. Murty, High Temperature Wear Behavior of Al-4Cu-TiB_2 In Situ Composites, *Wear*, 2010, **268**, p 1266–1274
31. Y. Zhang, N. Ma, H. Wang, Y. Le, and X. Li, Damping Capacity of In Situ TiB_2 Particulates Reinforced Aluminium Composites with Ti Addition, *Mater. Des.*, 2007, **28**, p 628–632
32. Y. Zhang, N. Ma, and H. Wang, Effect of particulate/Al interface on the damping behavior of in situ TiB_2 reinforced aluminium composite, *Mater. Lett.*, 2007, **61**, p 3273–3275
33. R. Shobha, K.R. Suresh, H.B. Niranjan, and K.G. Satyanarayana, Achieving Enhanced Mechanical Properties and Analysis of Chemical Kinetics of the In-Situ Reaction in an Al-TiB_2 In-situ Composite, *Adv. Mater. Res.*, 2010, **131**, p 1385–1388
34. H.B.M. Rajan, S. Ramabalan, I. Dinaharan, and S.J. Vijay, Effect of TiB_2 Content and Temperature on Sliding Wear Behavior of AA7075 / TiB_2 In Situ Aluminum Cast Composites, *Arch. Civ. Mech. Eng.*, 2014, **14**, p 72–79
35. M. Wang, D. Chen, Z. Chen, Y. Wu, F. Wang, N. Ma, and H. Wang, Mechanical Properties of In-Situ TiB_2/A356 Composites, *Mater. Sci. Eng. A*, 2014, **590**, p 246–254
36. Z. Chen, T. Wang, Y. Zheng, Y. Zhao, H. Kang, and L. Gao, Development of TiB_2 Reinforced Aluminum Foundry Alloy Based In Situ Composites: Part I: An Improved Halide Salt Route to Fabricate Al-5 wt.%TiB_2 Master Composite, *Mater. Sci. Eng. A*, 2014, **605**, p 301–309
37. J. Yao, S. Zhong, Z. Lei, and Z. Huoping, Mechanical Properties of Al-Si Alloy Based Composites Reinforced by In-Situ TiB_2 Particles, *Adv. Mater. Res.*, 2010, **105**–**106**, p 126–129
38. N.L. Yue, L. Lu, and M.O. Lai, Application of Thermodynamic Calculation in the In-Situ Process of Al/TiB_2, *Compos. Struct.*, 1999, **47**, p 691–694
39. B. Yang, Y.Q. Wang, and B.L. Zhou, The Mechanism of Formation of TiB_2 Particulates Prepared by In Situ Reaction in Molten Aluminum, *Met. Mater. Trans. B*, 1998, **29**, p 635–640
40. D. Zhao, X. Liu, Y. LiU, and X. Bian, In Situ Preparation of Al Matrix Composites Reinforced by TiB_2 Particles and Sub-micron ZrB_2, *J. Mater. Sci.*, 2005, **40**, p 4365–4368
41. L. Lu, M. La, and F.L. Chen, Al-4 wt% Cu Composite Reinforced with In-Situ TiB_2 Particles, *Acta Mater.*, 1997, **45**, p 4297–4309
42. Z.Y. Chen, Y.Y. Chen, Q. Shu, and G.Y. An, Solidification and Interfacial Structure of In Situ Al-4.5Cu/TiB_2 Composite, *J. Mater. Sci.*, 2000, **5**, p 5605–5608
43. A. Mandal, R. Maiti, M. Chakraborty, and B.S. Murty, Effect of TiB_2 Particles on Aging Response of Al-4Cu Alloy, *Mater. Sci. Eng. A*, 2004, **386**, p 296–300
44. C.F. Feng and L. Froyen, Microstructures of In Situ Al/TiB_2 MMCs Prepared, *J. Mater. Sci.*, 2000, **5**, p 837–850
45. B.S. Murty, R. Maiti, and M. Chakraborty, Development of In-Situ Al-TiB_2 Metal Matrix Composites, *J. Met. Mater. Sci.*, 2001, **43**, p 93–101
46. K.L. Tee, L. Lu, and M.O. Lai, In Situ Processing of Al-TiB_2 Composite by the Stir-Casting Technique, *J. Mater. Proc. Tech.*, 1999, **90**, p 513–519
47. K.L. Tee, L. Lu, and M.O. Lai, In Situ Stir Cast Al-TiB_2 Composite: Processing and Mechanical Properties, *Mater. Sci. Tech.*, 2001, **17**, p 201–206
48. K.L. Tee, L. Lu, and M.O. Lai, Synthesis of In Situ Al-TiB_2 Composites Using Stir Cast Route, *Compos. Struct.*, 2000, **47**, p 589–593
49. A. Changizi, A. Kalkanli, and N. Sevinc, Production of In Situ Aluminum: Titanium Diboride Master Alloy Formed by Slag-Metal Reaction, *J. Alloys Compd.*, 2011, **509**, p 237–240
50. L. Anestiev, L. Froyen, and L.V.A.N. Vugt, Kirkendall Effect in Liquid During the In Situ Processing of Metal Matrix Composites Under Micro-gravity Conditions, *J. Mater. Sci.*, 2002, **7**, p 1907–1913
51. M.F. Forster, R.W. Hamilton, R.J. Dashwood, and P.D. Lee, Centrifugal Casting of Aluminium Containing In Situ Formed TiB_2, *Mater. Sci. Technol.*, 2003, **19**, p 1215–1219
52. C. Dengbin, Z. Yutao, L.I. Guirong, Z. Meng, and C. Gang, Mechanism and Kinetic Model of In-situ TiB_2/7055Al Nanocomposites Synthesized Under High Intensity Ultrasonic Field, *J. Wuhan Univ. Technol. Mater. Sci. Ed.*, 2011, **26**, p 920–925
53. C.S. Ramesh, A. Ahamed, B.H. Channabasappa, and R. Keshavamurthy, Development of Al 6063-TiB_2 In Situ Composites, *Mater. Des.*, 2010, **31**, p 2230–2236
54. Z. Liu, Q. Han, J. Li, and W. Huang, Effect of Ultrasonic Vibration on Microstructural Evolution of the Reinforcements and Degassing of In Situ TiB_2p/Al-12Si-4Cu Composites, *J. Mater. Process. Technol.*, 2012, **212**, p 365–371
55. T. Wang, Z. Chen, Y. Zheng, Y. Zhao, H. Kang, and L. Gao, Development of TiB_2 Reinforced Aluminum Foundry Alloy Based In Situ Composites: Part II: Enhancing the Practical Aluminum Foundry Alloys Using the Improved Al-5 wt.%TiB_2 Master Composite Upon Dilution, *Mater. Sci. Eng. A*, 2014, **605**, p 22–32
56. I.G. Siddhalingeshwar, M.A. Herbert, M. Chakraborty, and R. Mitra, Effect of Mushy State Rolling on Age-Hardening and Tensile Behavior of Al-4.5Cu Alloy and In Situ Al-4.5Cu-5TiB_2 Composite, *Mater. Sci. Eng. A*, 2011, **528**, p 1787–1798
57. M.A. Herbert, C. Sarkar, R. Mitra, and M. Chakraborty, Microstructural Evolution, Hardness, and Alligatoring in the Mushy State Rolled Cast Al-4.5Cu Alloy and In-Situ Al4.5Cu-5TiB_2 Composite, *Metall. Mater. Trans. A*, 2007, **38**, p 2110–2126
58. J. Xue, J. Wang, Y.F. Han, and B.D. Sun, Wear Behaviour of Squeeze-Cast Al 2014 Alloy and In-Situ 5 vol% TiB_2/2014 Composite, *Mater. Trans.*, 2014, **53**, p 2119–2128
59. H. Yi, N. Ma, X. Li, Y. Zhang, and H. Wang, High-Temperature Mechanics Properties of In Situ TiB_{2p} Reinforced Al-Si Alloy Composites, *Mater. Sci. Eng. A*, 2006, **419**, p 12–17
60. D.G. Zhao, X.F. Liu, Y.C. Pan, Y.X. Liu, and X.F. Bian, Microstructure and Mechanical Behavior of AlSiCuMgNi Piston Alloys Reinforced with TiB_2, *J. Mater. Sci.*, 2006, **41**, p 4227–4232
61. C.S. Ramesh, S. Pramod, and R. Keshavamurthy, A Study on Microstructure and Mechanical Properties of Al 6061-TiB_2 In-Situ Composites, *Mater. Sci. Eng. A*, 2011, **528**, p 4125–4132
62. F. Wang, N. Ma, Y. Li, X. Li, and H. Wang, Impact Behavior of In Situ TiB_2/Al Composite at Various Temperatures, *J. Mater. Sci.*, 2011, **46**, p 5192–5196
63. F. Wang, J. Xu, J. Li, X. Li, and H. Wang, Fatigue Crack Initiation and Propagation in A356 Alloy Reinforced with In Situ TiB_2 Particles, *Mater. Des.*, 2012, **33**, p 236–241
64. Y. Zhang, N. Ma, H. Wang, Y. Le, and S. Li, Effect of Ti on the Damping Behavior of Aluminum Composite Reinforced with In Situ TiB_2 Particulate, *Scripta Mater.*, 2005, **53**, p 1171–1174

65. K. Sivaprasad, S.P.K. Babu, S. Natarajan, R. Narayanasamy, B.A. Kumar, and G. Dinesh, Study on Abrasive and Erosive Wear Behaviour of Al 6063/TiB_2 In Situ Composites, *Mater. Sci. Eng. A*, 2008, **498**, p 495–500
66. S. Natarajan, R. Narayanasamy, S.P. Kumaresh Babu, G. Dinesh, B. Anil Kumar, and K. Sivaprasad, Sliding Wear Behaviour of Al 6063/TiB_2 In Situ Composites at Elevated Temperatures, *Mater. Des.*, 2009, **30**, p 2521–2531
67. C.S. Ramesh and A. Ahamed, Friction and Wear Behaviour of Cast Al 6063 Based In Situ Metal Matrix Composites, *Wear*, 2011, **271**, p 1928–1939
68. Y. Birol, In Situ Synthesis of Al-TiCp Composites by Reacting K_2TiF_6 and Particulate Graphite in Molten Aluminium, *J. Alloys Compd.*, 2008, **454**, p 110–117
69. R. Bauri, Synthesis of Al-TiC In-Situ Composites: Effect of Processing Temperature and Ti:C Ratio, *Trans. Indian Inst. Met.*, 2009, **62**, p 391–395
70. A. Sharma, Synthesis of TiC Composite by Salt Route and Grain Refinement of Aluminium Alloy, *Int. J. Cast Metals Res.*, 2008, **21**, p 226–230
71. B. Sirahbizu, D. Venkateswarlu, M.M. Mahapatra, P.K. Jha, and N.R. Mandal, On Friction Stir Butt Welding of Al-12Si/10 wt% TiC In Situ Composite, *Mater. Des.*, 2014, **54**, p 1019–1027
72. R.N. Rai, A.K.P. Rao, G.L. Dutta, and M. Chakraborty, Forming Behaviour of Al-TiC In-situ Composites, *Mater. Sci. Forum*, 2013, **765**, p 418–422
73. P. Sahoo and M.J. Koczak, Analysis of In Situ Formation of Titanium Carbide in Aluminum Alloys, *Mater. Sci. Eng. A*, 1991, **144**, p 37–44
74. F. Wang, H. Liu, and B. Yang, Effect of In-Situ TiC Particulate on the Wear Resistance of Spray-Deposited 7075 Al Matrix Composite, *Mater. Char.*, 2005, **54**, p 446–450
75. Y. Cho, J. Lee, H. Kim, J. Kim, and S. Kim, Feasible Process for Producing In Situ Al/TiC Composites by Combustion Reaction in an Al Melt, *Met. Mater. Int.*, 2013, **19**, p 1109–1116
76. B. Yang, F. Wang, H. Cui, X.J. Duan, S.C. Hu, and J.S. Zhang, TiC Particulate-Reinforced Al-20Si-5Fe Composite Fabricated by Melt In Situ Reaction Spray Forming, *J. Mater Proc. Technol.*, 2003, **137**, p 187–190
77. Y.F. Liang, J.E. Zhou, and S.Q. Dong, Microstructure and Tensile Properties of In Situ TiCp/Al-4.5 wt.% Cu Composites Obtained by Direct Reaction Synthesis, *Mater. Sci. Eng. A*, 2010, **527**, p 7955–7960
78. Z. Liu, X. Wang, and Q. Han, Synthesis of Submicrometer-Sized TiC Particles in Aluminum Melt at Low Melting Temperature, *J. Mater. Res.*, 2014, **29**, p 896–901
79. R. Tyagi, Synthesis and Tribological Characterization of In Situ Cast Al-TiC Composites, *Wear*, 2005, **259**, p 569–576
80. A. Kumar, P.K. Jha, and M.M. Mahapatra, Abrasive Wear Behavior of In Situ TiC Reinforced with Al-4.5%Cu Matrix, *J. Mater. Eng. Perf.*, 2014, **23**, p 743–752
81. A. Kumar, M.M. Mahapatra, and P.K. Jha, Modeling the Abrasive Wear Characteristics of In-Situ Synthesized Al-4.5% Cu/TiC Composites, *Wear*, 2013, **306**, p 170–178
82. R.N. Rai, G.L. Datta, M. Chakraborty, and A.B. Chattopadhyay, A Study on the Machinability Behaviour of Al-TiC Composite Prepared by In Situ Technique, *Mater. Sci. Eng. A*, 2006, **428**, p 34–40
83. K. Tian, Y. Zhao, L. Jiao, S. Zhang, Z. Zhang, and X. Wu, Effects of In Situ Generated ZrB_2 Nano-particles on Microstructure and Tensile Properties of 2024Al Matrix Composites, *J. Alloys Compd.*, 2014, **594**, p 1–6
84. I. Dinaharan, N. Murugan, and S. Parameswaran, Influence of In Situ Formed ZrB_2 Particles on Microstructure and Mechanical Properties of AA6061 Metal Matrix Composites, *Mater. Sci. Eng. A*, 2011, **528**, p 5733–5740
85. S. Zhang, Y. Zhao, G. Chen, and X. Cheng, Microstructures and Dry Sliding Wear Properties of In Situ (Al_3Zr + ZrB_2)/Al Composites, *J. Mater. Proc. Technol.*, 2007, **184**, p 201–208
86. G.N. Kumar, R. Narayanasamy, S. Natarajan, S.P.K. Babu, K. Sivaprasad, and S. Sivasankaran, Dry Sliding Wear Behaviour of AA 6351-ZrB_2 In Situ Composite at Room Temperature, *Mater. Des.*, 2010, **31**, p 1526–1532
87. Q. Zheng and R.G. Reddy, Mechanism of In Situ Formation of AlN in Al Melt Using Nitrogen Gas, *J. Mater Sci.*, 2004, **9**, p 141–149
88. Q. Zheng and R.G. Reddy, Kinetics of In-Situ Formation of AlN in Al Alloy Melts by Bubbling Ammonia Gas, *Metall. Mater. Trans. B.*, 2003, **34**, p 793–804
89. Y. Huashun, J.D. Kim, and S.B. Kang, The Formation of AlN and TiN Particles During Nitrogen Bearing Gas Injection into Al-Mg-Ti Melt, *Mater. Sci. Eng. A*, 2004, **386**, p 318–325
90. S.S.S. Kumari, U.T.S. Pillai, and B.C. Pai, Synthesis and Characterization of In Situ Al-AlN Composite by Nitrogen Gas Bubbling Method, *J. Alloys Compd.*, 2011, **509**, p 2503–2509
91. S. Fale, A. Likhite, and J. Bhatt, Nucleation Criteria for the Formation of Aluminum Nitride in Aluminum Matrix by Nitridation, *Trans. Indian Inst. Met.*, 2013, **66**, p 265–271
92. K. Wang, C. Cui, Q. Wang, Y. Qi, and C. Wang, Fabrication of In Situ AlN-TiN/Al Inoculant and Its Refining Efficiency and Reinforcing Effect on Pure Aluminum, *J. Alloys Compd.*, 2013, **547**, p 5–10
93. H. Wang, Y. Zhao, G. Li, and Z. Zhang, Characterization of (Al_2O_3)p/Al Composites In Situ Synthesized by Direct Melt Reaction Method, *Adv. Mater. Res.*, 2011, **153**, p 25–28
94. B. Yang, M. Sun, G. Gan, C. Xu, Z. Huang, H. Zhang, and Z. Zak, In Situ Al_2O_3 Particle-Reinforced Al and Cu Matrix Composites Synthesized by Displacement Reactions, *J. Alloys Compd.*, 2010, **494**, p 261–265
95. M. Hoseini and M. Meratian, Fabrication of In Situ Aluminum–Alumina Composite with Glass Powder, *J. Alloys Compd.*, 2009, **471**, p 378–382
96. P.C. Maity, P.N. Chakraborty, and S.C. Panigrahi, Al-Al_2O_3 In Situ Particle Composites by Reaction of CuO Particles in Molten Pure Al, *Mater. Lett.*, 1997, **30**, p 147–151
97. P.C. Maity, P.N. Chakraborty, and S.C. Panigrahi, Preparation of Al-Al_2O_3 In-Situ Particle Composites by Addition of Fe_2O_3 Particles to Pure Al Melt, *J. Mater. Sci. Lett.*, 1997, **6**, p 1224–1226
98. B.S.S. Daniel and V.S.R. Murthy, Directed Melt Oxidation and Nitridation of Aluminium Alloys: A Comparison, *Mater. Des.*, 1995, **16**, p 155–161
99. V.S.R. Murthy and B.S. Rao, Microstructural Development in the Directed Melt-Oxidized (DIMOX) AI-Mg-Si Alloys, *J. Mater Sci.*, 1995, **30**, p 3091–3097
100. Y. Zhang, N. Ma, and H. Wang, Improvement of Yield Strength of LM24 Alloy, *J. Mater. Des.*, 2014, **54**, p 14–17
101. D. Ko, G. Yu, J. Youn, and Y. Kim, Ultrasonic Effect on Refinement of Mg_2Si and Mechanical Properties of In Situ Al-Mg_2Si Composites, *Adv. Mater. Res.*, 2009, **82**, p 549–552
102. R. Hadian, M. Emamy, N. Varahram, and N. Nemati, The Effect of Li on the Tensile Properties of Cast Al-Mg_2Si Metal Matrix Composite, *Mater. Sci. Eng. A*, 2008, **490**, p 250–257
103. N. Liu, J. Li, and H. Li, Influence of Sb on Wear Resistance of In-Situ Mg_2Si/Al-Si Composites, *Adv. Mater. Res.*, 2011, **313**, p 197–200
104. M. Emamy, H.R.J. Nodooshan, and A. Malekan, The Microstructure, Hardness and Tensile Properties of Al-15% Mg_2Si In Situ Composite with Yttrium Addition, *Mater. Des.*, 2011, **32**, p 4559–4566
105. R. Khorshidi, A.H. Raouf, M. Emamy, and H.R.J. Nodooshan, The Evolution of Heat Treatment on the Tensile Properties of Na-Modified Al-Mg_2Si In Situ Composite, *Adv. Mater. Res.*, 2011, **313**, p 283–286
106. B. Cicek, H. Ahlatci, and Y. Sun, Wear Behaviours of Pb Added Mg-Al-Si Composites Reinforced with In Situ Mg_2Si Particles, *Mater. Des.*, 2013, **50**, p 929–935
107. Y. Zhao, Q. Qin, Y. Zhao, Y. Liang, and Q. Jiang, In Situ Mg_2Si/Al-Si Composite Modified by K_2TiF_6, *Mater. Lett.*, 2004, **58**, p 2192–2194
108. J. Zhang, Z. Fan, Y.Q. Wang, and B.L. Zhou, Microstructural Evolution of the In Situ Al-15 wt.% Mg_2Si Composite with Extra Si Contents, *Scripta Mater.*, 2000, **42**, p 1101–1106
109. J. Zhang, Z. Fan, Y. Wang, and B. Zhou, Microstructural Refinement in Mg_2Si In Situ Composites, *J. Mater. Sci. Let.*, 1999, **8**, p 783–784
110. J. Zhang, Y. Zhao, X. Xu, and X. Liu, Effect of Ultrasonic on Morphology of Primary Mg_2Si in In-Situ Mg_2Si/Al Composite, *Trans. Nonferr. Soc. China*, 2013, **23**, p 2852–2856
111. H. Ahlatci, A. Durmaz, A. Balta, M. Acarer, and E. Candan, Effect of Ti on the Corrosion Behaviour of In-Situ Mg_2Si Particle Reinforced Al-12Si-20Mg-XTi Alloys Element Al Ti Si Mg, *Mater. Sci. Forum*, 2010, **637**, p 511–516
112. M. Emamy, R. Khorshidi, and A.H. Raouf, The Influence of Pure Na on the Microstructure and Tensile Properties of Al-Mg_2Si Metal Matrix Composite, *Mater. Sci. Eng. A*, 2011, **528**, p 4337–4342

113. M. Emamy, A.R. Emami, R. Khorshidi, and M.R. Ghorbani, The Effect of Fe-Rich Intermetallics on the Microstructure, Hardness and Tensile Properties of Al-Mg_2Si Die-Cast Composite, *Mater. Des.*, 2013, **46**, p 881–888
114. E. Georgatis, A. Lekatou, A.E. Karantzalis, H. Petropoulos, S. Katsamakis, and A. Poulia, Development of a Cast Al-Mg2Si-Si In Situ Composite: Microstructure, Heat Treatment, and Mechanical Properties, *J. Mater. Eng. Perf.*, 2013, **22**, p 729–741
115. A. Malekan, M. Emamy, J. Rassizadehghani, and A.R. Emami, The Effect of Solution Temperature on the Microstructure and Tensile Properties of Al-15% Mg_2Si Composite, *Mater. Des.*, 2011, **32**, p 2701–2709
116. Y. Sun and H. Ahlatci, Mechanical and Wear Behaviors of Al-12Si-XMg Composites Reinforced with In Situ Mg_2Si Particles, *Mater. Des.*, 2011, **32**, p 2983–2987
117. X. Lin, C. Liu, and H. Xiao, Fabrication of Al-Si-Mg Functionally Graded Materials Tube Reinforced with In Situ Si/Mg_2Si Particles by Centrifugal Casting, *Compos. Part B*, 2013, **45**, p 8–21
118. Y.G. Zhao, Q.D. Qin, Y.H. Liang, W. Zhou, and Q.C. Jiang, Mg_2Si/Al-Si-Cu Composite Modified by Strontium, *J. Mater Sci.*, 2005, **40**, p 1831–1833
119. R. Hadian, M. Emamy, and J. Campbell, Modification of Cast Al-Mg_2Si Metal Matrix Composite by Li, *Metall. Mater. Trans. B*, 2009, **40**, p 822–832
120. N. Soltani, A. Bahrami, and M.I. Pech-canul, The Effect of Ti on Mechanical Properties of Extruded In-Situ Al-15% Mg_2Si Composite, *Metall. Mater. Trans. A*, 2013, **44A**, p 4366–4373
121. W.U. Xiaofeng, Z. Guang, W.U. Fufa, and W. Zhe, Influence of Neodymium Addition on Microstructure, Tensile Properties and Fracture Behavior of Cast Al-Mg_2Si Metal Matrix Composite, *J. Rare Earths*, 2013, **31**, p 307–312